# ASCA OBSERVATIONS OF LMC SNRS



NASA Grant NAG5-2684

Final Report

For the Period 1 September 1994 through 31 August 1997

Principal Investigator
Dr. John P. Hughes

January 1999

Prepared for:

National Aeronautics and Space Administration
Goddard Space Flight Center
Greenbelt, Maryland 20771

Smithsonian Institution
Astrophysical Observatory
Cambridge, Massachusetts 02138

The Smithsonian Astrophysical Observatory
is a member of the
Harvard-Smithsonian Center for Astrophysics

The NASA Technical Officer for this grant is Dr. Nicholas White, Code 668, Laboratory for High Energy Astrophysics, NASA/Goddard Space Flight Center, Greenbelt, Maryland 20771.

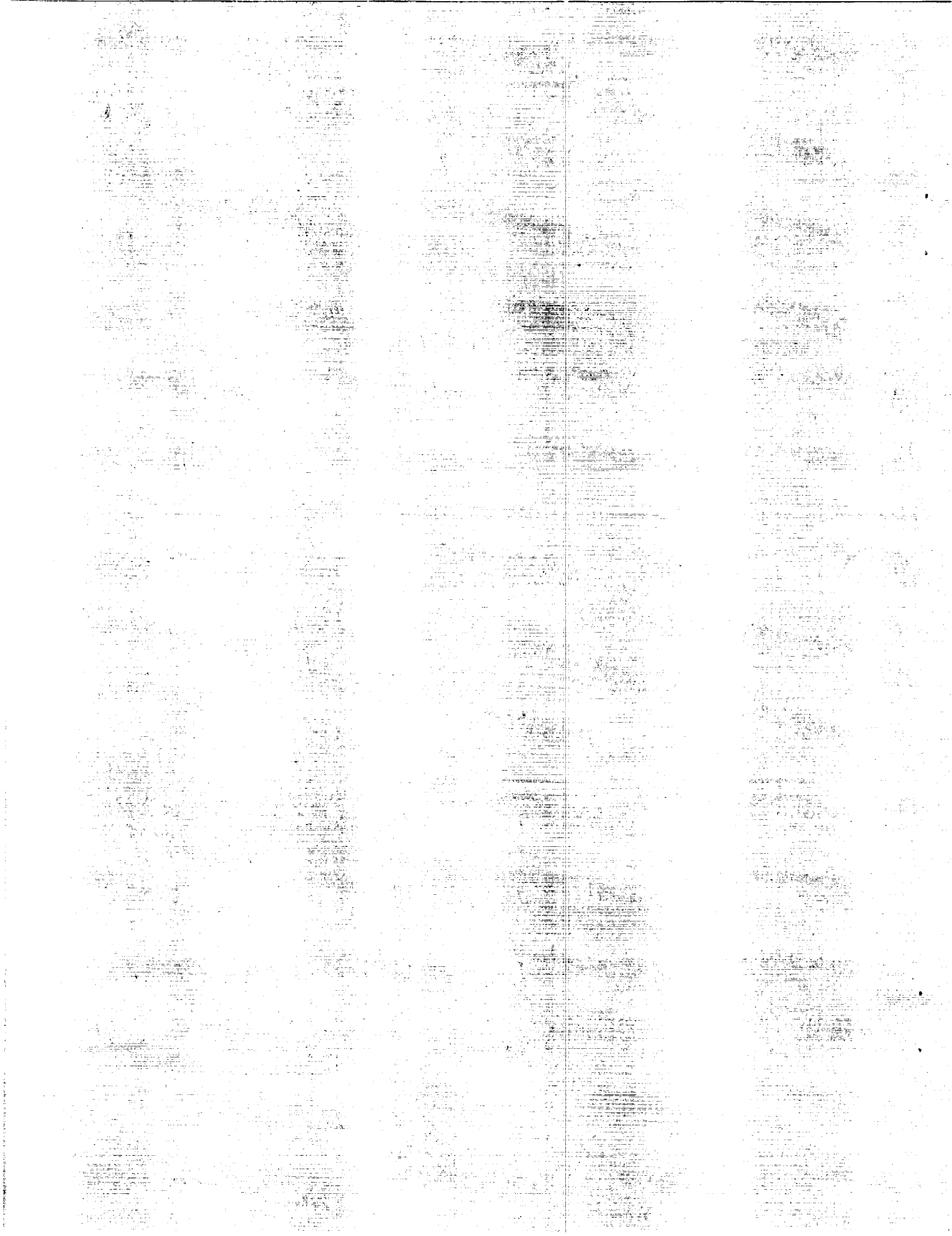

The following listed publications (also attached) serve as the final report for NASA Grant No. NAG5-2684

1.) "*ASCA* Observations of the Large Magellanic Cloud Supernova Remnant Sample: Typing Supernovae from Their Remnants," J. P. Hughes, I. Hayashi, D. J. Helfand, U. Hwang, M. Itoh, R. P. Kirshner, K. Koyama, T. H. Markert, H. Tsunemi, and J. Woo, ApJ, **444**, L81–L84, 1995.

2.) "*ASCA* X-ray Spectroscopy of LMC Supernova Remnants and the Metal Abundances of the LMC," J P. Hughes, I. Hayashi, and K. Koyama, ApJ, **505**, 732–748, 1998.

THE ASTROPHYSICAL JOURNAL, 444:L81–L84, 1995 May 10


# *ASCA* OBSERVATIONS OF THE LARGE MAGELLANIC CLOUD SUPERNOVA REMNANT SAMPLE: TYPING SUPERNOVAE FROM THEIR REMNANTS

JOHN P. HUGHES,[1] ICHIZO HAYASHI,[2] DAVID HELFAND,[3] UNA HWANG,[4] MASAYUKI ITOH,[5] ROBERT KIRSHNER,[1] KATSUJI KOYAMA,[2] THOMAS MARKERT,[6] HIROSHI TSUNEMI,[7] AND JONATHAN WOO[6]

*Received 1994 December 22; accepted 1995 February 22*

## ABSTRACT

We present our first results from a study of the supernova remnants (SNRs) in the Large Magellanic Cloud (LMC) using data from *ASCA*. The three remnants we have analyzed to date, 0509−67.5, 0519−69.0, and N103B, are among the smallest, and presumably also the youngest, in the Cloud. The X-ray spectra of these SNRs show strong Kα emission lines of silicon, sulfur, argon, and calcium with no evidence for corresponding lines of oxygen, neon, or magnesium. The dominant feature in the spectra is a broad blend of emission lines around 1 keV which we attribute to *L*-shell emission lines of iron. Model calculations (Nomoto, Thielemann, & Yokoi 1984) show that the major products of nucleosynthesis in Type Ia supernovae (SNs) are the elements from silicon to iron, as observed here. The calculated nucleosynthetic yields from Type Ib and II SNs are shown to be qualitatively inconsistent with the data. We conclude that the SNs which produced these remnants were of Type Ia. This finding also confirms earlier suggestions that the class of Balmer-dominated remnants arise from Type Ia SN explosions. Based on these early results from the LMC SNR sample, we find that roughly one-half of the SNRs produced in the LMC within the last ~1500 yr came from Type Ia SNs.

*Subject headings:* galaxies: individual (Large Magellanic Cloud) — nuclear reactions, nucleosynthesis, abundances — supernova remnants — X-rays: ISM

## 1. INTRODUCTION

A total of 32 supernova remnants (SNRs) have been identified in the Large Magellanic Cloud (LMC) based on observations at optical, radio, and X-ray wavelengths (Mathewson et al. 1983, 1984, 1985). The remnants range in diameter from 2 pc up to about 100 pc and span the range of known evolutionary phases, from young ejecta-dominated remnants, through middle-aged Sedov-type remnants, to old remnants in the radiative or snowplow phase. Twenty-seven of the LMC remnants emit X-rays at a detectable level ($F_X \gtrsim 5 \times 10^{-13}$ ergs s$^{-1}$ cm$^{-2}$ in the 0.15–4.5 keV band), while at least 11 are bright enough ($F_X \gtrsim 1 \times 10^{-11}$ ergs s$^{-1}$ cm$^{-2}$) for detailed X-ray spectroscopic study with *ASCA*. Most of these bright remnants have been observed already by *ASCA*: three during the performance verification phase and five during the first six months of the guest observer program by our collaboration. One of our goals for the LMC SNR sample is to find and study young, ejecta-dominated remnants. In this presentation we discuss results from preliminary analysis of data from three such remnants, 0509−67.5, 0519−69.0, and N103B.

Optically, N103B consists of several small bright knots which show the usual set of emission lines seen in most supernova remnants: [O III] λ5007, [S II] λλ6716, 6731, Hα, and so on (Danziger & Leibowitz 1985). The abundances of N103B inferred from optical spectroscopy are quite similar to those from other considerably larger and more evolved LMC remnants such as N63A and N49 (Russell & Dopita 1990). A high-resolution X-ray image of the remnant showed a spatial extent of only 3 pc radius, with a centrally peaked morphology (Mathewson et al. 1983). The X-ray spectrum appears to be thermal in nature (Singh et al. 1987), although detailed analysis was limited by the poor spectral resolution of these proportional counter data. The X-ray luminosity in the 0.15–4.5 keV band is $1.5 \times 10^{37}$ ergs s$^{-1}$, assuming a distance to the LMC of 50 kpc which we adopt throughout.

SNR 0519−69.0 belongs to a class of SNRs which show only hydrogen emission lines in their optical spectra with virtually no emission from collisionally excited forbidden lines. The prototypical Balmer-dominated SNR is the remnant of SN 1572 observed by Tycho Brahe, which is believed to be a Type Ia SN based on its historical light curve. The interpretation of the optical spectrum from the remnant in the context of a model in which a high-velocity nonradiative shock overtakes neutral interstellar gas (Chevalier, Kirshner, & Raymond 1980) allows for the independent determination of the SN shock velocity. For remnants in the LMC, this provides crucial information for constraining the age of the SNR. Analysis of the Balmer-dominated optical spectrum of 0519−69.0 indicates a shock velocity of 1000–1900 km s$^{-1}$, which, when combined with a radial size of 3.6 pc, makes the remnant 750–1500 years old (Smith et al. 1991). The high-resolution X-ray image of this remnant shows a nearly circular shell of emission that correlates very well with the Hα emission (Mathewson et al. 1983). Except for its broadband luminosity ($8.9 \times 10^{36}$ ergs s$^{-1}$), no other information concerning its X-ray spectrum was available before *ASCA*.

The third remnant in our sample, 0509−67.5, is also Balmer-dominated. Smith et al. (1991) obtained only a lower limit to the shock velocity of 2000 km s$^{-1}$; when combined

[1] Harvard-Smithsonian Center for Astrophysics, 60 Garden Street, Cambridge, MA 02138.
[2] Department of Physics, Kyoto University, Kitashirakawa, Oiwake-cho, Sakyo-ku, Kyoto 606, Japan.
[3] Astronomy Department, Columbia University, 538 W. 120 Street, New York, NY 10027.
[4] NASA/Goddard Space Flight Center, Code 666, Greenbelt, MD 20771.
[5] Institute for Space and Astronautical Science, 1-1, Yoshinodai 3-chome, Sagamihara, Kanagawa 229, Japan.
[6] Center for Space Research and Department of Physics, Massachusetts Institute of Technology, 70 Vassar Street, Cambridge, MA 02139.
[7] Department of Physics, Osaka University, 1-1, Machikaneyama-cho, Toyonaka, Osaka 560, Japan.

with the remnant's radius (3.3 pc), this sets an upper limit to the age of 1000 yr. The soft X-ray luminosity is $2.8 \times 10^{36}$ ergs $s^{-1}$.

The Balmer-dominated remnants (0509−67.5 and 0519−69.0) are particularly important because Tuohy et al. (1982) have suggested that they arise from the explosions of Type Ia SNs. As we show below, our *ASCA* data confirm this suggestion by observing directly the expected products of nucleosynthesis from such SNs.

## 2. DATA ANALYSIS

SNRs 0509−67.5, 0519−69.0, and N103B were observed on 1993 November 10, 8, and 9, respectively, by the X-ray astronomy satellite *ASCA* (Tanaka, Inoue, & Holt 1994). The data discussed here are from the two CCD detectors (Solid-state Imaging Spectrometer SIS0 and SIS1) and were obtained in the "1-CCD faint" mode of operation. We used the FTOOLS software package developed by the *ASCA* Guest Observer Facility for the following reduction procedures. The data were converted from faint to bright mode, hot pixels in the CCD were identified and removed using the CLEANSIS algorithm and the source light curves were searched for count rate excesses or flares (none were found). Events with grades 0, 2, 3, 4 were extracted from a circular region with radius ~4′ centered on the target.

The broad point-spread-function of the *ASCA* X-ray telescope makes determining an appropriate background spectrum extremely difficult, since the source flux from an unresolved object, such as we have here, extends over most of the CCD chip. In this analysis, background was estimated from areas of the detector away from the source, but from within the same chip. At about 1 keV, roughly 5% of the target flux was included in the background spectrum and this fraction increased to ~20% at 4 keV. Although this effect does not compromise our results here, it does cause a reduction in the intensity of the higher energy emission relative to that at lower energy. This should be kept in mind when assessing the significance of line features in our spectra.

The net effective exposure times were $3.3 \times 10^4$ s, $2.3 \times 10^4$ s, and $1.9 \times 10^4$ s, and the average background-subtracted count rates per SIS were 0.18 $s^{-1}$, 0.59 $s^{-1}$, and 0.92 $s^{-1}$, for SNRs 0509−67.5, 0519−69.0, and N103B, respectively. Figure 1 shows the *ASCA* spectra for the three remnants where, for presentation purposes only, the data from SIS0 and SIS1 have been summed.

There are several notable aspects of our *ASCA* spectra. First is the general similarity among the spectral features present. The dominant feature is a broad smooth blend of emission peaking between 0.7 and 1 keV which we identify as the unresolved complex of iron *L*-shell lines. Over roughly the same energy range, *K*-shell line emission from highly ionized ions of oxygen, neon, and magnesium is conspicuously absent, while at higher energies we clearly see prominent K$\alpha$ emission from He-like ions of silicon, sulfur, argon, and (excepting SNR 0509−67.5) calcium. If we merely use the relative intensities of the observed lines as an indicator of the relative elemental abundances, our data suggest that the abundances of silicon, sulfur, argon, calcium, and iron are considerably enhanced relative to those of oxygen, neon, and magnesium. Additional quantitative support for this argument is presented in § 3 below.

Model fits were performed to gain some insight into the average thermodynamic state of the X-ray emitting gas in these SNRs. A parametric model consisting of a thermal bremsstrahlung continuum, Gaussian lines, and interstellar X-ray absorption was used. Figure 1 shows the best-fit models superposed on the data. The fitted continuum temperatures were quite

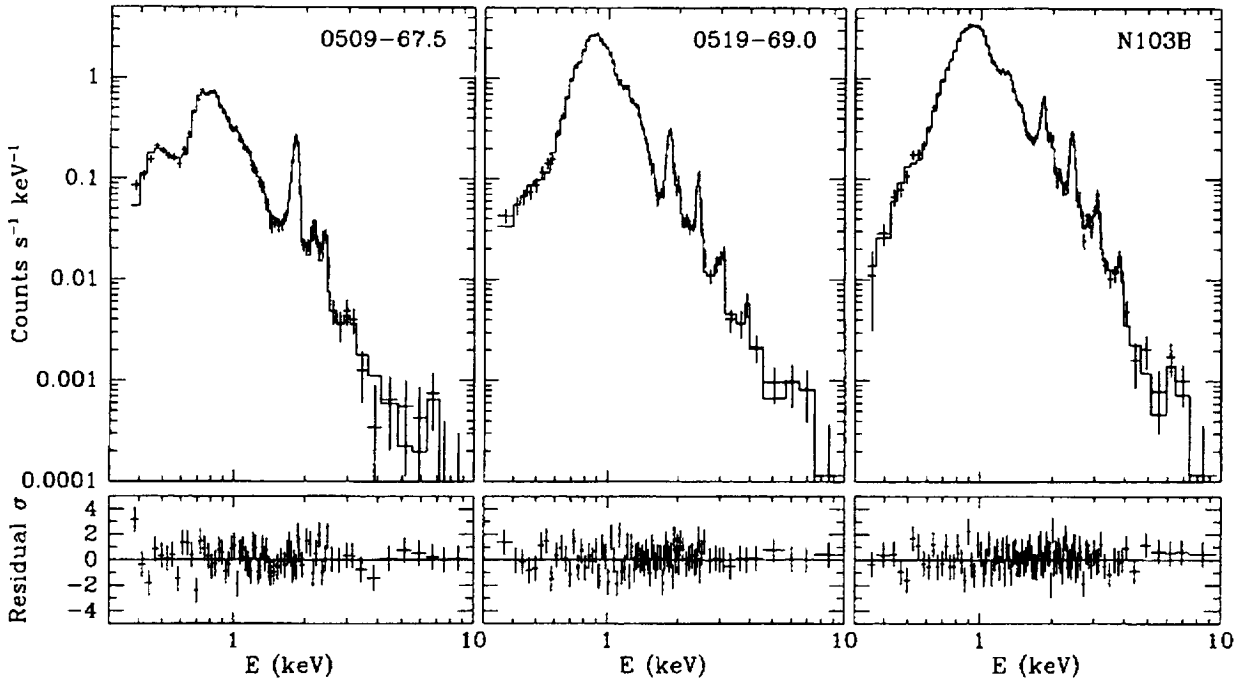


FIG. 1.—*ASCA* X-ray spectra of three LMC SNRs: 0509−67.5, 0519−69.0, and N103B. The data have been background subtracted and the spectra from both sensors have been added. Note that the background dominates the source spectrum at energies greater than about 5 keV. Energy channels were grouped so that each bin contained at least 25 counts in the raw spectrum. The best-fit parametric model for each source is shown as the histogram. The small panels at the bottom indicate the difference between the data and model in terms of the statistical error in each channel. Although we have included a narrow emission line in the fits around 6.5 keV, the interpretation of this as Fe K$\alpha$ line emission from the SNRs is highly uncertain due to the presence of strong instrumental background fluorescence lines of Fe and Ni in this energy band.

similar: $1.24 \pm 0.20$, $1.48 \pm 0.13$, and $1.13 \pm 0.06$ keV for 0509−67.5, 0519−69.0, and N103B, respectively. This quantity was constrained mainly by the shape of the continuum above ~1.4 keV. We derived an ionization state indicator by taking the ratio of intensities of the silicon hydrogen-like to helium-like Kα lines. The ratios obtained, $\lesssim 0.02$, 0.22, and 0.37, correspond to ionization timescales, $n_e t$, of $\lesssim 10^{10.4}$, $10^{11.2}$, and $10^{11.4}$ cm$^{-3}$ s (assuming the best-fit continuum temperatures derived above), when the nonequilibrium ionization (NEI) model of Hughes & Singh (1994) is employed. This sequence of increasing level of ionization from 0509−67.5 to N103B, is qualitatively consistent with the observed increase in the mean energy of the iron *L*-shell blend along the same sequence. We note that the lowest ionization timescale we measure is close to the value known for the 400 yr old remnant of Tycho's SN (Hughes 1991). The larger values for the other remnants are still far from equilibrium ionization ($n_e t \sim 10^{12.5}$ cm$^{-3}$ s).

## 3. DISCUSSION

Simulations using the NEI plasma emission model were performed to interpret the observed line ratios. We assumed the mean temperature ($kT = 1.28$ keV) and ionization timescale ($n_e t = 10^{11}$ cm$^{-3}$ s) from the parametric fits. However, our conclusions are not sensitive to this choice and any single set of values derived above would yield essentially the same results. A column density of $2 \times 10^{21}$ atoms cm$^{-2}$, appropriate for sources in the LMC, was assumed. Detailed NEI fits and parameter estimation are underway, but, at the present time, results are limited by uncertainties in the background subtraction, instrumental calibrations, and the atomic physics required to model the X-ray emission. Figure 2 presents simulated *ASCA* SIS spectra for three cases which we discuss below.

The leftmost panel of Figure 2 shows the *ASCA* SIS spectrum expected from a plasma with mean LMC abundances (roughly 0.3 times cosmic). Strong iron *L*-shell emission around 1 keV is apparent in the model spectrum. However, the prominent Kα emission lines of oxygen, neon, and magnesium, on the one hand, and the relatively weak Kα emission lines from the higher atomic number elements on the other, are inconsistent with our data and argue strongly against a swept-up ISM interpretation of our X-ray spectra.

The middle panel of Figure 2 assumes a plasma with abundances corresponding to the ejecta from a 25 $M_\odot$ core-collapse SN (Type II SN). During the normal course of their evolution, massive stars produce large amounts of O-group elements which are ejected during the SN explosion. Numerical models for the nucleosynthetic yield as a function of progenitor mass have been calculated by Thielemann, Nomoto, & Hashimoto (1994), Woosley (1991), and others. In general, these models predict that the ejecta of Type II SNs should contain an overabundance of the O-group elements relative to Si and the elements beyond. Recent analysis of archival X-ray spectral data for the oxygen-rich SNR G292.0+1.8 (Hughes & Singh 1994) has confirmed these general abundance patterns for at least one massive-star core-collapse SN. The *ASCA* X-ray spectrum of the young oxygen-rich SNR 0102.2−72.2 in the Small Magellanic Cloud (Hayashi et al. 1994) has revealed strong line emission from O, Ne, and Mg and thus is qualitatively consistent with having arisen from a core-collapse SN. Because the *ASCA* spectral data from the three remnants presented here show no emission from O-group elements, it is clear that they did not originate as Type II SNs.

The origin of Type Ib SNs remains somewhat controversial. Two models are currently popular: off-center detonations in accreting white dwarfs or core collapse in massive Wolf-Rayet stars which have lost their hydrogen envelopes. Optical observations of these SNs at late times show strong oxygen line emission and consequently both classes of progenitor model have been developed in order to produce ejecta containing large amounts of oxygen (Woosley, Taam, & Weaver 1986; Ensman & Woosley 1988), which makes them inconsistent with our X-ray data.

The abundance distribution for the ejecta of a Type Ia SN has been determined by Nomoto et al. (1984) assuming that these events arise from the carbon deflagration of a C+O

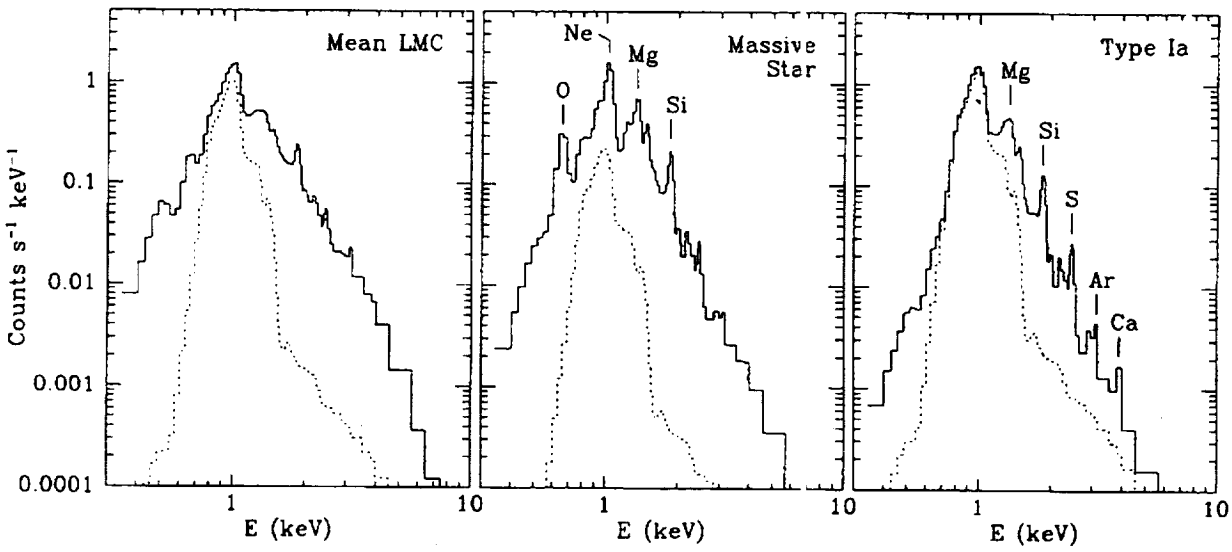


FIG. 2.—NEI spectral models for three possible sets of elemental abundances. The left panel shows a model spectrum assuming a plasma with the mean abundances of the LMC (0.3 times cosmic), the middle panel assumes a plasma with abundances corresponding to the ejecta from a massive-star core-collapse SN (the 25 $M_\odot$ case from Thielemann et al. 1994), and the right panel assumes the abundance distribution in the ejecta of a Type Ia SN (the "W7" model of Nomoto et al. 1984). All cases employ a single-temperature, single-ionization-timescale NEI model with $kT = 1.28$ keV and $n_e t = 10^{11}$ cm$^{-3}$ s. The emission from Fe is shown separately as the dotted curve. Prominent Kα emission lines from the various elemental species are indicated.

TABLE 1

THE SMALLEST SUPERNOVA REMNANTS IN THE LARGE MAGELLANIC CLOUD

| SNR Name | Age or Radius | SN Type |
|---|---|---|
| SN 1987A ..... | 8 yr | II |
| 0540−69.3..... | 1.5 pc | II |
| N157B ..... | 1.8 pc | (II)? |
| N103B ..... | 3.0 pc | Ia |
| 0509−67.5..... | 3.3 pc | Ia |
| 0519−69.0..... | 3.6 pc | Ia |

white dwarf. The dominant ejecta products according to these calculations are Si, S, Ar, Ca, and Fe. The simulated SIS spectrum based on this model (rightmost panel of Fig. 2) clearly shows emission line features from these species with an absence of strong O and Ne emission. Our observed spectra bear a remarkable resemblance to this model spectrum. Thus we conclude, based on the *ASCA* spectral data, that the three remnants under study here arose from Type Ia SN explosions.

In Table 1 we list the six SNRs in the LMC with X-ray diameters less than 10 pc (Mathewson et al. 1983). Four of these have good age estimates: SN 1987A, of course, is 8 yr old, 0540−593 is between 700 and 1100 yr old (Reynolds 1985; Kirshner et al. 1989), and 0509−67.5 and 0519−69.0 are both less than 1500 yr old (Smith et al. 1991). We assume, based on their small sizes, that N157B and N103B are also younger than 1500 yr. These six remnants indicate a SN rate in the LMC of 1.4 SN per century per $10^{10}$ $L_\odot$ (assuming $L_B$ for the LMC is $2.8 \times 10^9$ $L_\odot$).

We have argued above that three of the remnants in Table 1 are products of Type Ia SNs. The three remaining young remnants are almost certainly the product of massive star explosions: for N157B and 0540−693, the dominant X-ray and radio emission have the characteristics of pulsar-driven, Crab-like remnants, and in the latter, we see the pulsar itself (as well as oxygen-rich ejecta); the progenitor of the third, SN 1987A was directly observed to be a massive star. These results indicate that the ratio of Type Ia to Type II (+Ib) SNs in the LMC is approximately 1:1 based on the sample of remnants younger than 1500 yr.[8]

In their review of SN rates, van den Bergh & Tammann (1991) find this ratio to be 1:10 for galaxies of Hubble type Sdm–Im, although this value is based on a very small number of observed events, and assumes a galaxy inclination correction for Type II events only which more recent work has cast into doubt (van den Bergh 1994); assuming that no factor is required to correct for events missed in edge-on galaxies, the adopted ratio would fall to 1:5. van den Bergh & Tammann (1991) also discuss explicitly the expected rates of different SN types in the LMC. The massive star-formation rate and the expected SN rate from extragalactic patrols converge on a Type II value of $2 \times 10^{-3}$ per year. The Type Ia rate is discussed both in terms of the extragalactic observations, and the ratio of nova rate to SN Ia rate; the expected value for the LMC in both cases is $\sim 5 \times 10^{-4}$ per year.

The results presented here favor an even higher rate of Type Ia events relative to massive star explosions (we reject a ratio of 1:4 or smaller at 90% confidence, assuming Poisson statistics). It is possible that observational selection effects have militated against the discovery of some young SNRs from Type II SNs, those which, for example, might have exploded in heavily absorbed regions or in low-density superbubbles. However, this is unlikely to be the complete explanation since the Type II (+Ib) SN rate based on the remnants in Table 1 is fully consistent with the expected rate. It is the absolute Type Ia rate which appears too high: observing at least three events in 1500 years when the mean rate is 1 per 2000 years has a Poisson probability of only 4%.

## 4. CONCLUSIONS

In this article we have presented new *ASCA* X-ray spectral data for three small SNRs in the LMC. We find that the X-ray spectra are dominated by emission from the astrophysically abundant elements from silicon to iron. Emission from oxygen, neon, and magnesium is relatively much weaker. This leads us to conclude, based on comparison to model predictions of the nucleosynthesis expected from the various types of SNs, that all three remnants are the products of Type Ia SNs. Since two of the remnants are classified as having Balmer-dominated optical spectra, our results confirm earlier suggestions (Tuohy et al. 1982) that such remnants arise from Type Ia SNs.

When examined in the context of the LMC SNR sample in general, we are led to the conclusion that the ratio of rates of Type I to Type II (+Ib) SNs is nearly 1:1. Furthermore we find that it is the absolute rate of Type Ia SN which appears higher than expected based on statistical samples of SNs in late-type galaxies. These observations have interesting implications for the nature of the progenitors of Type Ia SNs as well as for the chemical evolution of the LMC.

This research was partially supported by NASA grant NAG5-2684 to the Smithsonian Institution.

[8] Some slight correction to this ratio may be required to account for known LMC remnants which are larger than 10 pc in diameter, but may be younger than 1500 yr (N132D is one possible example, see Hughes 1987).

## REFERENCES

Chevalier, R. A., Kirshner, R. P., & Raymond, J. C. 1980, ApJ, 235, 186
Danziger, I. J., & Leibowitz, E. M. 1985, MNRAS, 216, 365
Ensman, L. M., & Woosley, S. E. 1988, ApJ, 333, 754
Hayashi, I., Koyama, K., Ozaki, M., Miyata, E., Tsunemi, H., Hughes, J. P., & Petre, R. 1994, PASJ, 46, L121
Hughes, J. P. 1987, ApJ, 314, 103
———. 1991, in Supernovae, The Tenth Santa Cruz Summer Workshop in Astronomy and Astrophysics, ed. S. Woosley (Berlin: Springer), 661
Hughes, J. P., & Singh, K. P. 1994, ApJ, 422, 126
Kirshner, R. P., Morse, J. A., Winkler, P. F., & Blair, W. P. 1989, ApJ, 342, 260
Mathewson, D. S., Ford, V. L., Dopita, M. A., Tuohy, I. R., Long, K. S., & Helfand, D. J. 1983, ApJS, 51, 345
Mathewson, D. S., Ford, V. L., Dopita, M. A., Tuohy, I. R., Mills, B. Y., & Turtle, A. J. 1984, ApJS, 55, 189
Mathewson, D. S., Ford, V. L., Tuohy, I. R., Mills, B. Y., Turtle, A. J., & Helfand, D. J. 1985, ApJS, 58, 197
Nomoto, K., Thielemann, F.-K., & Yokoi, K. 1984, ApJ, 286, 644
Reynolds, S. P. 1985, ApJ, 291, 152
Russell, S. C., & Dopita, M. A. 1990, ApJS, 74, 93
Singh, K. P., Westergaard, N. J., Schnopper, H. W., & Helfand, D. J. 1987, ApJ, 322, 80
Smith, R. C., Kirshner, R. P., Blair, W. P., & Winkler, P. F. 1991, ApJ, 375, 652
Tanaka, Y., Inoue, H., & Holt, S. S. 1994, PASJ, 46, L37
Thielemann, F.-K., Nomoto, K., & Hashimoto, M. 1994, in Supernovae, Les Houches, Session LIV, ed. S. Bludman, R. Mochkovitch, & J. Zinn-Justin (North-Holland: Elsevier Sci. Pub.), 629
Tuohy, I. R., Dopita, M. A., Mathewson, D. S., Long, K. S., & Helfand, D. J. 1982, ApJ, 261, 473
van den Bergh, S. 1994, preprint
van den Bergh, S., & Tammann, G. A. 1991, ARA&A, 29, 363
Woosley, S. E. 1991, in Supernovae, The Tenth Santa Cruz Summer Workshop in Astronomy and Astrophysics, ed. S. Woosley (Berlin: Springer), 202
Woosley, S. E., Taam, R. E., & Weaver, T. A. 1986, ApJ, 301, 601

THE ASTROPHYSICAL JOURNAL, 505:732–748, 1998 October 1


# *ASCA* X-RAY SPECTROSCOPY OF LARGE MAGELLANIC CLOUD SUPERNOVA REMNANTS AND THE METAL ABUNDANCES OF THE LARGE MAGELLANIC CLOUD

JOHN P. HUGHES
Department of Physics and Astronomy, Rutgers University, 136 Frelinghuysen Road, Piscataway, NJ 08854-8019; jph@physics.rutgers.edu

AND

ICHIZO HAYASHI AND KATSUJI KOYAMA
Department of Physics, Graduate School of Science, Kyoto University, Sakyo-ku, Kyoto 606-8502, Japan; hayashi@cr.scphys.kyoto-u.ac.jp, koyama@cr.scphys.kyoto-u.ac.jp
*Received 1998 February 26; accepted 1998 May 7*

## ABSTRACT

We present the results of X-ray spectroscopy of a flux-limited sample of seven middle-aged supernova remnants (SNRs) in the Large Magellanic Cloud (LMC): N23, N49, N63A, DEM 71, N132D, 0453−68.5, and N49B. We constructed self-consistent nonequilibrium ionization SNR models assuming a Sedov solution for the dynamical evolution, and then applied the resulting spectral models to the data obtained by the Solid State Imaging Spectrometer on board the *Advanced Satellite for Cosmology and Astrophysics*. All the remnants were reasonably well described by the model, which allowed us to derive accurate values for their physical parameters, i.e., ages, densities, initial explosion energies, and metal abundances. The derived explosion energies vary from $5 \times 10^{50}$ to $6 \times 10^{51}$ ergs. A restricted subset of the sample exists for which the ionization and Sedov dynamical ages agree quite well under the assumption that the electron and ion temperatures are not fully equilibrated at the shock front; for these four SNRs, the mean value of the initial explosion energy is $(1.1 \pm 0.5) \times 10^{51}$ ergs. We show that it is likely that the other three remnants, all of which have inferred explosion energies $\gtrsim 3 \times 10^{51}$ ergs, exploded within preexisting cavities in the interstellar medium. The limits on high-energy X-ray emission ($\gtrsim 3$ keV) that we present indicate that these SNRs do not contain very luminous pulsar-powered synchrotron nebulae, in general agreement with our picture of them as evolved, middle-aged remnants. We find statistical evidence for enrichment by supernova ejecta in the sense that smaller remnants show a somewhat higher mean metallicity than the larger ones. In the case of DEM 71, the putative remnant of a Type Ia supernova, the derived abundance of iron is about a factor of 2 larger than the other remnants in the sample. These things being said, however, the derived abundances are in general dominated by swept-up interstellar material, and so we use the SNR sample to estimate the mean LMC gas-phase abundances. We find that the astrophysically common elements from oxygen to iron are less abundant than the solar values by factors of 2–4. Overall, these results are consistent with previous ones based on optical and UV data but do not show the anomalous overabundance of magnesium and silicon seen by others.

*Subject headings:* galaxies: abundances — ISM: abundances — Magellanic Clouds — nuclear reactions, nucleosynthesis, abundances — supernova remnants — X-rays: ISM

## 1. INTRODUCTION

Studies of the supernova remnants (SNRs) in the Large Magellanic Cloud (LMC) are essential for elucidating the details of SNR evolution, nucleosynthesis, the nature and environments of supernova progenitors, and so on. As probes of the interstellar medium (ISM), SNRs also yield information on the energy balance and chemical composition of their environments, which serves as input to larger questions of galactic chemical evolution and the star formation history of the Cloud. The relative closeness of the LMC plus its well-determined distance (we use 50 kpc throughout) means that accurate physical quantities can be derived for individual remnants in the galaxy. Also, owing to the generally low interstellar absorption toward the LMC, it is possible to detect X-rays in the important 0.5–2.5 keV energy band, which includes emission lines from some of the most abundant metals in the universe, such as K-shell transitions of highly ionized atoms of oxygen, neon, magnesium, silicon, and sulfur and L-shell lines of ionized iron. The Solid State Imaging Spectrometer (SIS) on board the *Advanced Satellite for Cosmology and Astrophysics* (*ASCA*), with its superior energy resolution compared to previous broadband X-ray spectrometers, gives us the first real opportunity for studying these issues quantitatively in the X-ray regime.

Mathewson et al. (1983, 1984, 1985) identified 32 SNRs in the LMC on the basis of optical, radio, and X-ray observations. The remnants range in size from 2 pc to about 100 pc and therefore span the range of evolutionary phases, from young ejecta-dominated remnants, through middle-aged adiabatic remnants, to old remnants in the radiative phase. At least 12 of the LMC remnants are bright enough X-ray emitters ($F_X > 10^{-11}$ ergs s$^{-1}$ cm$^{-2}$ in the 0.15–4.5 keV band) that we can perform detailed spectroscopic study with *ASCA*. First results have already been reported from *ASCA* on three small LMC remnants, N103B, 0509−67.5, and 0519−69.0 (Hughes et al. 1995), that show strong emission lines originating from ejecta characteristic of thermonuclear supernovae, i.e., SNe Ia.

For the research described herein, we observed seven middle-aged remnants, N23, N49, N63A, DEM 71, N132D, 0453−68.5, and N49B, with *ASCA* and performed detailed

TABLE 1

*ASCA* OBSERVATION LOG OF LMC SNRs

| SNR | Other Name[a] | Date of Observation | Exposure Time (ks) | Source Count Rate[b] SIS0/SIS1 (counts $s^{-1}$) |
|---|---|---|---|---|
| 0453−68.5..... | ... | 1995 Nov 25 | 38.7 | 0.14/0.11 |
| 0505−67.9..... | DEM 71 | 1995 Oct 8 | 28.7 | 0.50/0.39 |
| 0506−68.0..... | N23 | 1993 Nov 9 | 32.9 | 0.35/0.29 |
| 0525−66.0..... | N49B | 1994 Oct 10 | 37.4 | 0.35/0.25 |
| 0525−66.1..... | N49 | 1994 Oct 10 | 37.4 | 0.59/0.55 |
| 0525−69.6..... | N132D | 1993 Sep 23 | 5.2 | 4.07/3.39 |
| 0535−66.0..... | N63A | 1993 Nov 21 | 18.0 | 3.16/2.62 |

[a] N: Henize 1956; DEM: Davies, Elliott, & Meaburn 1976.
[b] From within the source extraction regions.

spectral analysis of their SIS data. This is all the LMC SNRs larger than 5 pc (radius) and brighter than $10^{11}$ ergs $s^{-1}$ $cm^{-2}$ over the soft X-ray band, which includes the three brightest thermal X-ray–emitting remnants in the LMC (N132D, N63A, and N49), plus four less luminous ones that cover a range of evolutionary states. Previous X-ray spectroscopic studies of N49, N63A, N132D, and N49B were reported by Clark et al. (1982) based on Solid State Spectrometer (SSS) data from the *Einstein Observatory*. The SSS data clearly showed weak emission lines of Mg, Si, and S indicative of thermal emission, although the analysis, which used somewhat unphysical two-temperature collisional ionization equilibrium plasma models, left some doubt about the reliability of the derived elemental abundance values. More recently Hwang et al. (1993) analyzed all the available *Einstein* data on N132D using a phenomenological nonequilibrium ionization (NEI) model and derived abundances of the heavy elements that were considerably lower than the solar values. Both analyses suggest that the bulk of the X-ray emission from these remnants comes from swept-up ISM rather than supernova ejecta, and, as we show below, our *ASCA* data confirm this finding. This observational fact gives us confidence that the SNR abundances we measure indeed correspond to those of the ISM in the LMC.

The elemental abundances of the Magellanic Clouds are of great importance to extragalactic astronomy. As the nearest major galaxies to our own, they are well studied and serve as the stepping stones for studies of more distant systems. In the current chemical composition of the Clouds we see at least some of the material returned to the ISM by stars of all types through winds and supernovae, and, using models of stellar evolution and nucleosynthesis, we can constrain the history of star formation in these galaxies. It is well known that the Clouds have undergone quite different star formation histories from the Galaxy, based on their differing chemical properties (see, for example, Tsujimoto et al. 1995).

In the past 20 yr with the advent of high-quality optical and UV spectra, the study of the chemical abundances of the LMC has made great progress. The earlier results of this era (summarized in Dufour 1984) showed that the metallicity of LMC H II regions was significantly less than solar; the observed oxygen abundance, for example, was only about one-third the solar value. More recent studies (Luck & Lambert 1992; Russell & Dopita 1992, hereafter RD92) have, in general, tended to confirm these findings using optical spectra and detailed modeling of H II regions, SNRs, Cepheids, and supergiant stars in the LMC. However, even though considerable effort has been expended in this area of research over the past decade, there remains considerable room for improvement. In particular, certain critical elements, such as Mg and Si, are not easily studied in the optical and UV bands owing to a paucity of appropriate atomic transitions. The work we present here represents the first systematic attempt to measure the gas-phase LMC abundances in a new, independent manner using X-ray spectroscopy of SNRs.

Our spectral analysis also allows us, for the first time, to derive accurate values for the temperature, ionization timescale, and intrinsic X-ray emissivity of the hot gas in LMC SNRs. When combined with their physical radii, which are accurately known because of the well-established distance to the LMC, we have four independent observational constraints on the dynamical evolution. Only three of these quantities are necessary to specify fully the evolutionary state according to the Sedov (1959) similarity solution, so in fact the observational data result in an overconstrained system. This allows us to go beyond merely assuming the Sedov solution and instead allows us actually to establish whether or not the Sedov model is a correct representation for the evolution of the SNRs in our sample.

In the following we present our *ASCA* analysis of the selected LMC SNR sample. In § 2 we briefly present the observational details. In contrast to the phenomenological models used in previous X-ray studies of LMC SNRs, we have developed realistic self-consistent models that incorporate the dynamical evolution of remnants. Section 3 provides a description of the spectral model we developed and compares our calculations to similar published ones. Results of the Sedov model fits, as well as considerations of the applicability of the model, are given in § 4. Discussions of the derived abundances are in § 5. In § 6 we examine the high energy X-ray emission ($\gtrsim$3 keV) of the remnant sample. We comment on individual remnants in § 7 and summarize in the final section.

## 2. OBSERVATIONS

*ASCA* has four identical X-ray telescopes (XRTs) and four focal plane detectors. Two of the focal plane instruments are solid-state imaging spectrometers (SIS0 and SIS1; CCD cameras), and the other two are gas imaging spectrometers (GIS2 and GIS3; gas scintillation proportional counters). A summary of the *ASCA* observatory and its complement of instruments has been given by Tanaka, Inoue, & Holt (1994).

The log of observations for our remnant sample is given in Table 1. All but one of the remnants were observed

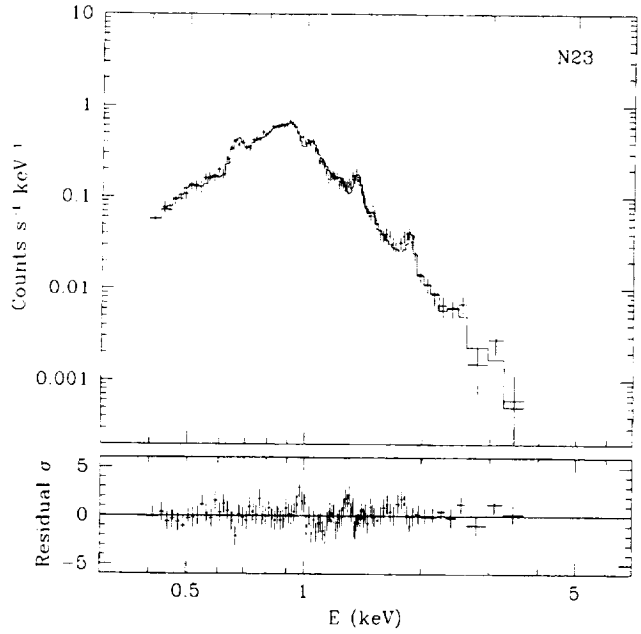


FIG. 1a

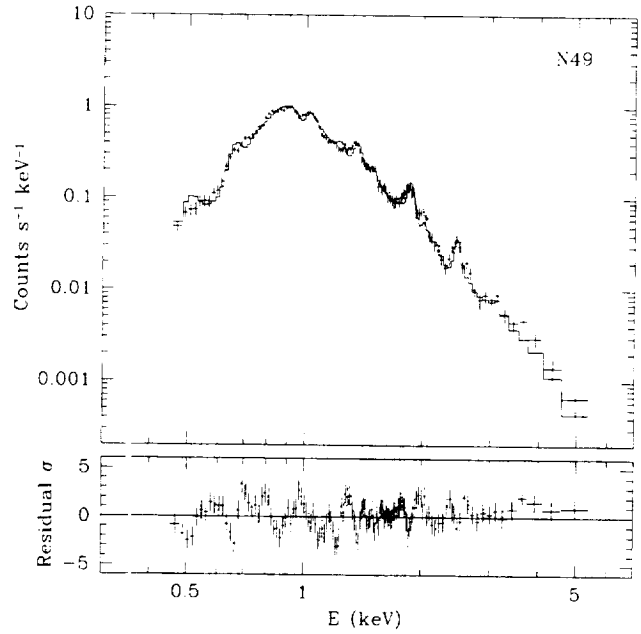


FIG. 1b

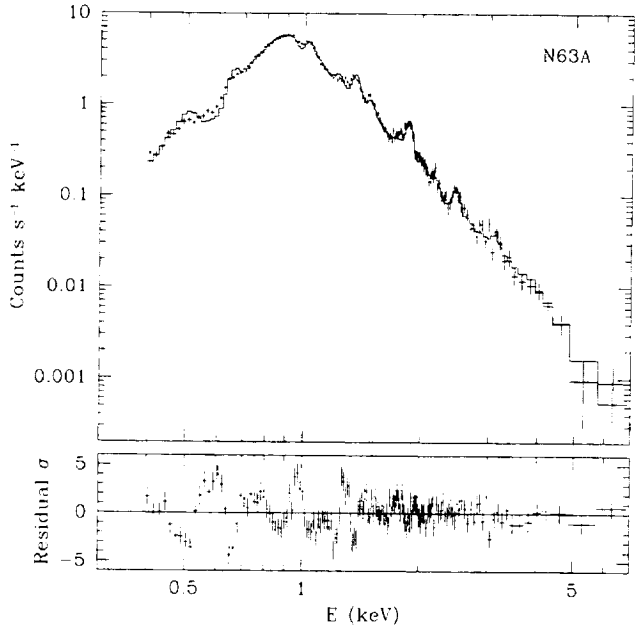


FIG. 1c

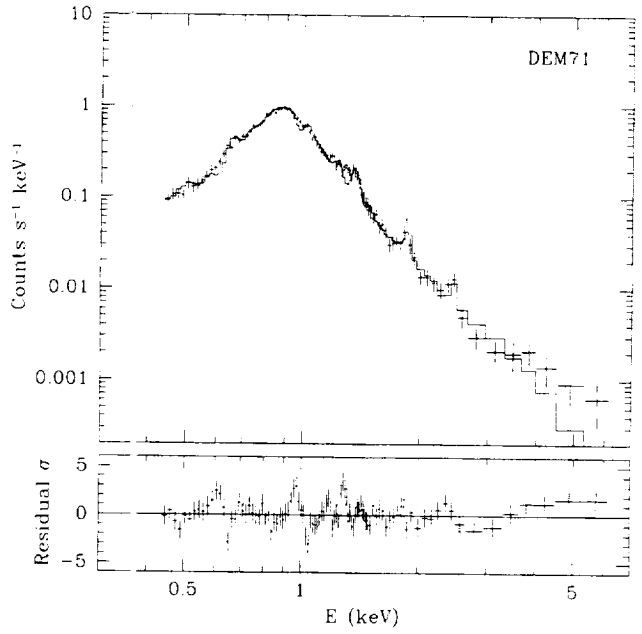


FIG. 1d

FIG. 1.—*ASCA* SIS spectra of seven LMC SNRs. In each panel the data and 1 $\sigma$ statistical errors are shown by the crosses. The solid histogram is the best-fit spectrum from the Sedov model assuming full electron-ion temperature equilibration. For clarity of display only, the SIS0 and SIS1 data and corresponding models were averaged. The actual spectral analysis was done by jointly fitting to both sets of SIS data.

during the Performance Verification phase or the first Guest Observer cycle. The seven remnants in our sample were all found to have soft spectra (mean electron temperatures $kT_e \lesssim 1$ keV), so we used only the SIS data for the present spectral analysis. The SIS was operated in 1-CCD faint mode for all observations. The data were corrected for dark-frame error, the echo effect, and charge-transfer inefficiency, and hot and flickering pixels were removed using standard procedures. Data were rejected during orbital times of high background (South Atlantic Anomaly passages) or when the geomagnetic cutoff rigidity was less than 6 GeV/c. In order to avoid contamination due to light leaks through the optical blocking filters, we excluded all data taken when the satellite viewing direction was 10° or less from the bright rim of the Earth. X-ray spectra were extracted from circular regions of radius 4′ centered on each SNR with the exception of N49 and N49B. Owing to their close relative proximity (N49 and N49B are separated on the sky by merely 6.7), the spectra of these two remnants were obtained from 3′ radius regions. In all cases, background spectra were constructed from source-free regions in the SIS field of view of the same observation. We

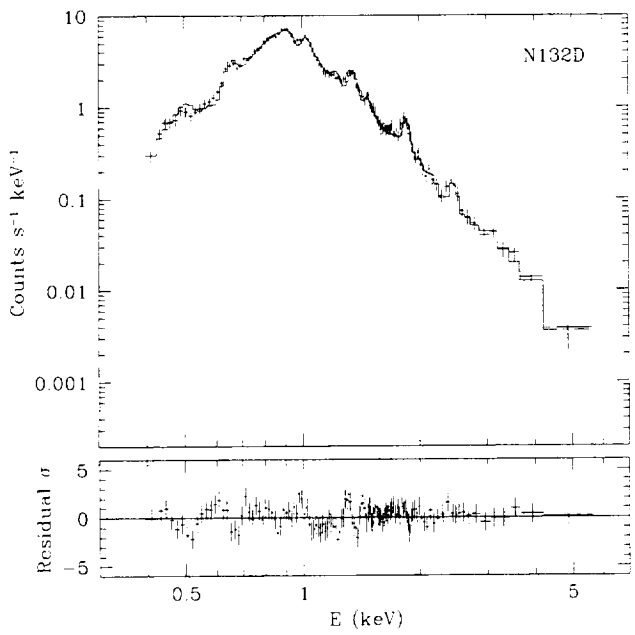


FIG. 1e

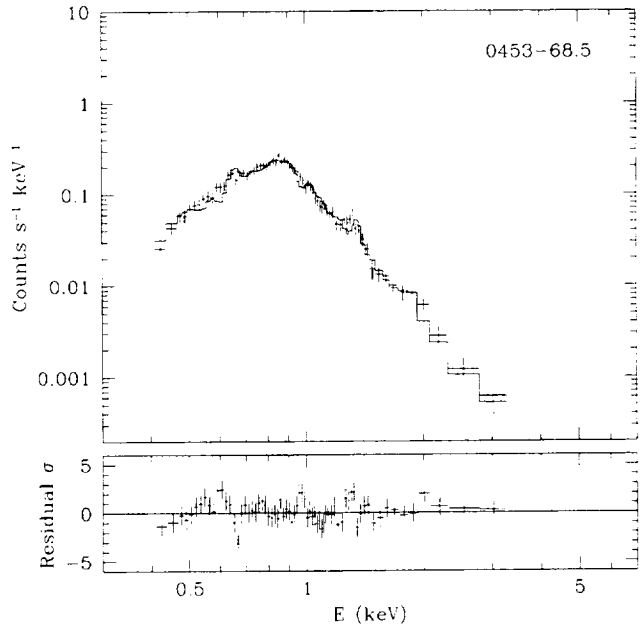


FIG. 1f

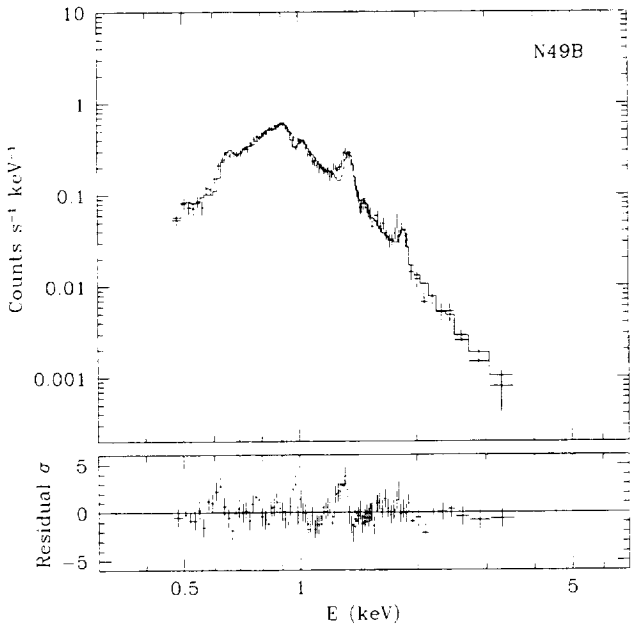


FIG. 1g

show the background-subtracted SIS0 spectra of our remnant sample in Figure 1.

## 3. SPECTRAL MODELS

### 3.1. *Phenomenological Model*

The X-ray spectra in Figure 1 are all clearly thermal in nature, showing characteristic K-shell line emission from highly ionized atoms of oxygen, neon, magnesium, silicon, and sulfur as well as a broad blend of iron L-shell emission near 1 keV. The spectra of the different SNRs are remarkably similar to each other, while they differ sharply from the young ejecta-dominated remnants that we studied in our earlier work on the LMC SNRs (Hughes et al. 1995). In fact, whereas the *ASCA* spectra of the ejecta-dominated SNRs appear qualitatively more consistent with an abundance distribution corresponding to SN Ia ejecta, the seven remnants in the current study are more consistent with the roughly one-third solar abundances of the LMC.

As our first approach to a quantitative analysis of these spectra, we used a phenomenological model, free from any specific dynamical model of SNR evolution, for including NEI effects in the spectral fitting (Hayashi et al. 1995). In this approach the X-ray–emitting plasma is assumed to have been shock heated some time ago $t$ to a constant temperature $T_e$. The ionization timescale, which is the parameter characterizing deviations from ionization equilibrium, is given by $n_e t$, where $n_e$ is the mean electron density. In simple terms these parameters are determined from the data in the following manner: $T_e$ is largely con-

strained by the shape of the continuum emission, while $n_e t$ is constrained by the emission-line ratios (principally the ratio of helium-like to hydrogen-like K$\alpha$ lines). In addition to the temperature and ionization timescale, the elemental abundances, an emission measure, and the line-of-sight absorption column density were required to specify the model completely. The code is based on the NEI model from Hughes & Helfand (1985); we use the implementation described in Hughes & Singh (1994).

No remnant could be adequately described by a single-component NEI plasma model, i.e., with one $T_e$ and $n_e t$ for all species. In particular, the degree of ionization appeared to vary from element to element. Similar discrepancies of this kind were found in fits of the phenomenological NEI plasma model to the *ASCA* data of the young oxygen-rich SNR 0102−72.3 in the Small Magellanic Cloud (Hayashi et al. 1994). We therefore modified our fits to the LMC SNRs to allow for variable ionization timescales for the different elemental species displaying prominent line emission in the observed band, while at the same time retaining a single value of $T_e$. This model provided improved fits, the results of which allowed us to estimate the quantity of X-ray–emitting plasma in the various SNRs. Assuming a constant density shell filling one-fourth of the entire volume, using the fitted elemental abundances (which were all substantially less than solar; Hayashi et al. 1995), and taking the remnant radii from Mathewson et al. (1983) (see also Table 2), we obtained masses ranging from several tens to several hundred solar masses. Clearly these are evolved remnants that have swept up a large quantity of ISM.

Nevertheless, the apparent dependence of $n_e t$ on elemental species as implied by this phenomenological NEI model makes us question its physical plausibility. Taken at face value, one interpretation of the ionization timescale variation might be that the various elemental species are in spatially disjoint zones that have undergone differing thermodynamic histories. Since the amount and approximate composition of the X-ray–emitting plasma are consistent with being dominated by ISM material (which should be chemically homogeneous), rather than SN ejecta (which may not be), we are confident that this explanation can be rejected. An alternate and indeed more physically plausible explanation is that the X-ray–emitting plasma is chemically homogeneous but contains a broad range of temperatures and ionization timescales. This situation would arise as a natural consequence of incorporating realistic models for the dynamical evolution of SNRs, since our spectra are integrated over the entire X-ray emission from each remnant. Apparent variation of the average value of $n_e t$ with composition, for example, would then arise as a result of the strong dependence of ionization, recombination, and excitation rates, as well as other atomic physics quantities, on elemental species. In effect, each species would tend to pick out that value of $n_e t$ that produces a maximum of intensity in the relevant emission lines. Some support for this scenario comes from the fact that, at least for N132D, a better fit to the *ASCA* data was obtained using a two-component phenomenological NEI model that contained emission from gas at both $\sim 0.5$ and $\sim 2$ keV (Hayashi 1997) (see § 7.5 below).

TABLE 2

SEDOV MODEL FITS TO LMC SNRs[a]

| SNR | $R$(pc) | $N_H(10^{21}\mathrm{cm}^{-2})$ | $kT_s$(keV) | log $n_0 t_s$(cm$^{-3}$ s) | $N_S(10^{12}\mathrm{cm}^{-5})$ | $n_0$(H cm$^{-3}$) | $t_s(10^3$ yr) | $E_0(10^{51}$ ergs) | $M_{ST}(M_\odot)$ |
|---|---|---|---|---|---|---|---|---|---|
| N23 | 6.7 | 0.8(0.3) | 0.53(0.10) | 10.89(0.27) | 0.33(0.12) | 1.6 | 3.8 | 0.46 | 70 |
| | | 0.7(0.3) | 0.59(0.15) | 11.16(0.21) | 0.35(0.10) | 1.7 | 3.6 | 0.53 | 70 |
| N49 | 8.2 | 2.2(0.3) | 0.58(0.05) | 11.33(0.18) | 1.59(0.28) | 2.6 | 4.4 | 1.5 | 210 |
| | | 2.1(0.3) | 0.62(0.05) | 11.52(0.13) | 1.57(0.24) | 2.6 | 4.3 | 1.6 | 200 |
| N63A | 8.5 | 1.4(0.1) | 0.62(0.04) | 11.23(0.17) | 3.77(0.55) | 3.9 | 4.5 | 2.6 | 330 |
| | | 1.4(0.2) | 0.68(0.07) | 11.38(0.13) | 3.95(0.49) | 3.9 | 4.2 | 2.9 | 340 |
| DEM 71 | 10.4 | 0.4(0.3) | 0.82(0.14) | 10.58(0.11) | 0.21(0.06) | 0.67 | 4.7 | 1.1 | 110 |
| | | 0.6(0.3) | 0.83(0.41) | 11.03(0.10) | 0.35(0.13) | 0.86 | 4.7 | 1.4 | 140 |
| N132D | 12.1 | 1.3(0.2) | 0.68(0.06) | 10.95(0.16) | 4.70(0.79) | 2.5 | 6.1 | 5.4 | 630 |
| | | 1.3(0.1) | 0.78(0.14) | 11.19(0.07) | 5.43(0.27) | 2.7 | 5.7 | 6.7 | 680 |
| 0453−68.5 | 15.0 | $<1.1$ | 0.51(0.14) | 10.68(0.30) | 0.12(0.07) | 0.30 | 8.7 | 0.91 | 140 |
| | | $<0.5$ | 0.70(0.39) | 11.01(0.34) | 0.11(0.05) | 0.28 | 7.4 | 1.2 | 130 |
| N49B | 17.0 | 2.6(0.4) | 0.41(0.06) | 10.78(0.11) | 1.15(0.57) | 0.75 | 10.9 | 2.7 | 520 |
| | | 2.5(0.4) | 0.44(0.10) | 11.08(0.16) | 1.37(0.55) | 0.82 | 10.6 | 3.1 | 560 |

| SNR | O | Ne | Mg | S | Si | Fe | $\chi^2$/d.o.f. | $L_X$[0.5 – 5 keV] ($10^{36}$ ergs s$^{-1}$) |
|---|---|---|---|---|---|---|---|---|
| N23 | 0.27(0.06) | 0.47(0.09) | 0.53(0.13) | 0.38(0.11) | 0.50(0.3[illegible]) | 0.31(0.08) | 1.4/172 | 2.5 |
| | 0.32(0.08) | 0.45(0.11) | 0.50(0.13) | 0.36(0.10) | 0.52(0.3[illegible]) | 0.28(0.07) | 1.3/172 | |
| N49 | 0.32(0.04) | 0.48(0.05) | 0.44(0.09) | 0.45(0.05) | 0.61(0.1[illegible]) | 0.29(0.05) | 2.4/247 | 6.3 |
| | 0.38(0.04) | 0.48(0.09) | 0.43(0.09) | 0.43(0.07) | 0.58(0.1[illegible]) | 0.29(0.05) | 2.5/247 | |
| N63A | 0.25(0.05) | 0.50(0.05) | 0.50(0.06) | 0.40(0.05) | 0.29(0.0[illegible]) | 0.31(0.04) | 2.8/146 | 20 |
| | 0.28(0.05) | 0.45(0.08) | 0.46(0.08) | 0.36(0.05) | 0.27(0.0[illegible]) | 0.30(0.04) | 2.7/146 | |
| DEM 71 | 0.22(0.03) | 0.55(0.08) | 0.50(0.12) | 0.26(0.09) | 0.47(0.2[illegible]) | 0.62(0.12) | 2.2/178 | 3.4 |
| | 0.27(0.05) | 0.48(0.08) | 0.39(0.11) | 0.24(0.08) | 0.57(0.2[illegible]) | 0.47(0.08) | 2.1/178 | |
| N132D | 0.21(0.03) | 0.44(0.06) | 0.46(0.07) | 0.34(0.05) | 0.36(0.11) | 0.30(0.04) | 1.8/229 | 30 |
| | 0.24(0.02) | 0.42(0.04) | 0.41(0.04) | 0.31(0.03) | 0.36(0.0[illegible]) | 0.27(0.02) | 1.8/229 | |
| 0453−68.5 | 0.21(0.05) | 0.28(0.07) | 0.33(0.13) | 0.23(0.14) | $<0.78$ | 0.26(0.08) | 2.1/121 | 0.98 |
| | 0.26(0.09) | 0.25(0.09) | 0.33(0.15) | 0.23(0.14) | $<0.71$ | 0.28(0.10) | 2.1/121 | |
| N49B | 0.22(0.03) | 0.42(0.05) | 0.74(0.10) | 0.28(0.06) | $<0.30$ | 0.21(0.04) | 2.5/169 | 3.2 |
| | 0.23(0.05) | 0.36(0.07) | 0.63(0.12) | 0.25(0.07) | $<0.39$ | 0.16(0.03) | 2.4/169 | |

[a] For each remnant, the results of fits with models assuming full electron and ion temperature equilibration are given in the upper line, while those from models assuming Coulomb equilibration timescales are given in the lower line. The distance to the LMC was taken to be 50 kpc. Values in parentheses represent the 90% confidence statistical errors.

### 3.2. *Sedov Model*

We consider the Sedov (1959) similarity solution for an adiabatic blast wave expanding into a uniform, homogeneous ISM as the description for the dynamical evolution of our SNRs. As is well known, this phase of evolution begins when the mass of swept-up ISM grows to be much more than the mass of SN ejecta (so that the ejecta are dynamically insignificant) (Gull 1973), and it lasts until radiative cooling becomes important, which occurs roughly when the shock temperature drops below $\sim 10^6$ K (Cox 1972). Based on our estimates of the swept-up mass from the phenomenological model fits, the seven LMC SNRs in the sample are all old enough that they satisfy the first constraint and thus are likely to be in the adiabatic phase of evolution. In § 4 below, we show that the remnants are not so old that radiative cooling has affected their dynamical evolution, and so they also satisfy the second condition.

In order to calculate the emergent NEI X-ray spectrum, the time history of the electron density and temperature throughout the model remnant is required. For this calculation we divided the remnant into a number of spherically symmetric shells spaced linearly in the nondimensional variable $V = u/(r/t)$, where $u$ and $r$ are the velocity and radial position of a specific shell, respectively, and $t$ is the remnant's age. This choice of integration variable ensures a fine spacing near the shock front where the emission measure of the remnant is the largest and the time variation of the relevant quantities is the most rapid. For simplicity, the time integration was constrained so that on successive time steps a single new spatial shell was shock heated and incorporated into the remnant. Consequently the more finely the remnant was divided spatially, the shorter was the time step. Based on some trial studies with the *ASCA* spectrum of N132D, it was found that 30 shells provided an optimal compromise between execution speed and calculational accuracy, and so this value was adopted for the analysis. The temperature and density of each interior shell at each time step was determined from the analytical expression for the interior variation of these quantities (Sedov 1959). It was assumed that the composition was spatially uniform and that hydrogen and helium were fully ionized. The mean molecular weight per particle was also assumed constant across the remnant, which is a good approximation for the low-metallicity environment of the LMC, where the gas is dominated by hydrogen and helium.

With the time dependence of the electron density and temperature now fully specified, the ionization rate equations were integrated using the matrix diagonalization method (see, e.g., Masai 1984; Hughes & Helfand 1985) to determine the final (observed) ionization state as a function of position. Then the radial run of temperature, coupled with the ionization state, was used to calculate the total emergent X-ray spectrum summed over the entire model SNR. We used the ionization and recombination rate coefficients and the X-ray emission code of Masai (1984). The unshocked ISM was assumed to be in ionization equilibrium at a temperature of $T = 3 \times 10^5$ K, but the final results are very insensistive to the precise value of this quantity. Again experiments with the spectrum of N132D found no significant difference in the best-fit parameters when the temperature defining the initial equilibrium ionization fractions was varied from $10^4$ to $10^6$ K. This is because ionization of the first few ion states proceeds very rapidly; most of the time is spent in the helium- and hydrogen-like ionic stages for the medium-$Z$ atomic species that are important in our analysis (i.e., the abundant elements from oxygen to sulfur, see below).

Emission from 13 elements (H, He, C, N, O, Ne, Mg, Si, S, Ar, Ca, Fe, and Ni) is included in our model. The abundances of helium and carbon cannot be determined from our data since there are no significant emission lines from these species in the *ASCA* X-ray band. Furthermore, we found that the abundances of nitrogen, argon, calcium, and nickel were not well constrained by the data. Consequently, we fixed the abundances of these elements to the LMC values determined by RD92: He 10.94, C 8.04, N 7.14, Ar 6.29, Ca 5.89, and Ni 6.04, where we quote values on a scale of 12 + log (M/H). The baseline abundances we assume for the other species are O 8.82, Ne 7.92, Mg 7.42, Si 7.52, S 7.2, and Fe 7.6, which are the cosmic values from Allen (1973, p. 31). The precise values of the carbon, nitrogen, argon, calcium, and nickel abundances have virtually no effect on our measurements of the other elemental abundances, unless the listed species are extremely overabundant relative to solar, which is unlikely, again given the low metallicity of the LMC. The helium abundance does have some impact on the absolute values of our derived abundances, since a significant fraction of the continuum emission (roughly 30% at 1 keV) is provided by helium. Roughly speaking a 10% increase (decrease) in the helium abundance translates into a 5%–10% increase (decrease) in the derived abundances of the other elements. On the other hand, the relative abundance values we derive are affected to a much lesser extent by changes in the helium abundance.

The parameters of the model are the shock temperature ($T_s$), the ionization timescale ($n_0 t_i$, where $n_0$ is the preshock ISM number density of hydrogen atoms and $t_i$ is the ionization age of the remnant), the abundances of the elements listed above, and a normalization factor ($N = n_0^2 \theta_R^3 D$, where $\theta_R$ and $D$ are the angular radius and distance of the remnant, respectively). The quantities $T_s$ and $n_0 t_i$ are constrained by the data in the same manner as described above for the phenomenological NEI model, and the normalization factor is essentially determined from the X-ray flux. When the radius of each remnant is included, we have four independent observational constraints on the three independent parameters of the Sedov model, namely age, ambient ISM density, and initial explosion energy. This overconstrained system allows us to carry out an internal check on whether or not the Sedov solution is a correct description of the SNRs in our sample. In effect what we do is to explore the consistency between the age derived from the dynamics of the Sedov model (which depends on $T_s$ and $\theta_R$) and that derived from the fitted ionization timescale (converted to an age using $n_0$ derived from the normalization factor). One complication is that none of the remnants in our sample displays the ideal, spherical symmetry expected of the Sedov model, so an additional multiplicative factor is needed to account for the fraction of volume within the radius of the remnant that is filled with X-ray emitting gas when the fitted normalization factor is converted to a mean density. The last parameter in the spectral fits is the line-of-sight absorbing column density $N_H$. We use the cross sections of Morrison & McCammon (1983).

The precise relationship between the amount of energy imparted to ions and electrons at supernova shock fronts is still one of the major unsolved issues in the physics of strong

collisionless shocks (Shklovsky 1968). Whether the electrons attain the same mean thermal velocity behind the shock front as the ions, in which case they will have a considerably lower temperature, or very rapidly equilibrate with the ions, as proposed by McKee (1974), is still not entirely clear. Therefore we have constructed two classes of models that encompass the plausible extremes of these possible situations. The first is a full equilibration model, where the electron and ion temperatures are assumed to be equal. The other model assumes that the electrons and ions attain the same mean thermal velocity at the shock and then share energy solely through Coulomb collisions (see Spitzer 1978) and that, consequently, the electron temperature lags the ion temperature (see, for example, Itoh 1978; Cox & Anderson 1982). However, as it turns out for our sample of LMC remnants, with the possible exception of the ionization timescale, the fitted parameters do not depend strongly on which model is assumed, and, in particular, the derived abundances are almost the same in the two models.

As part of our model verification, we computed a number of simple diagnostic quantities and compared our results with those from the similar Sedov-phase NEI models of Hamilton, Sarazin, & Chevalier (1983). We found reasonable agreement (within a factor $\simeq 2$) between the two models for the continuum flux at 2 keV, the He-like K$\alpha$ line flux, the Fe-L line flux, and the X-ray luminosity above 0.1 keV. Our model gives a slightly higher ionization state than the Hamilton et al. model, which is most likely due to the difference in the rate coefficients used by the models.

## 4. RESULTS OF SEDOV MODEL FITS

In Figure 1 we show the SIS spectra and the best-fit NEI spectral models for all the remnants in our sample. Sedov models assuming full electron-ion temperature equilibration are plotted; the other set of models assuming Coulomb temperature equilibration would be indistinguishable from these. For display purposes only we averaged the SIS0 and SIS1 data and corresponding best-fit spectral models. For the actual analysis, in all cases but one, both the SIS0 and SIS1 spectra were fitted jointly. The one exception is N63A, where there was a pronounced gain discrepancy for the SIS1 data. Rather than introducing an ad hoc gain correction, we decided to use only the SIS0 data for this SNR. Because of its high flux and reasonably long exposure (see Table 1), N63A has the best statistics of any remnant in the sample, and so the loss of the SIS1 data does not seriously impede our ability to determine its spectral parameters. In all cases the SIS data were rebinned so that each spectral channel contained at least 20 counts after background subtraction. This allows us to use $\chi^2$ as the figure-of-merit function for assessing goodness of fit and determining best-fit quantities and confidence levels. In Table 2, we give the best-fit values and 90% confidence level statistical uncertainties for the spectral parameters and elemental abundances for both the full equilibration model and the model assuming energy exchange between electron and ions through Coulomb collisions.

From a statistical point of view, the reduced $\chi^2$ values given in Table 2 are formally unacceptable. However, systematic errors in the experimental data due to calibration uncertainties, for example, have not been included, nor have we included uncertainties due to the atomic physics or the incompleteness of the X-ray line lists used in the spectral models. This last point is particularly important since the pattern of residuals for all the SNRs shows significant excesses at photon energies of $\sim 0.9$ keV and $\sim 1.2$ keV, which are due to missing Fe L-shell lines in the models. As a representation of the *ASCA* data, however, the Sedov model does a considerably better job than the phenomenological NEI model discussed above (§ 3.1), which was specifically introduced in order merely to reproduce the observed *ASCA* spectra with little astrophysical motivation. Although the phenomenological model requires a larger number of free parameters, the Sedov model provides fits with comparable or even better quality. Given our present state of knowledge of the instrumental calibration and the atomic physics of X-ray spectral line emission, we believe that the Sedov model describes the *ASCA* spectra about as well as can be expected.

Our fitted column densities from the *ASCA* spectra agree quite well with estimates of the total column toward each remnant based on the H I gas in the Galaxy (Heiles & Cleary 1979) and in the LMC (McGee & Milton 1966). In particular, the total column of H I gas is greatest toward N49, N63A, and N49B (values of $\sim 2.1 \times 10^{21}$ atoms cm$^{-2}$) and is least toward N23, DEM 71, N132D, and 0453−68.5 (values of $\sim 1.2 \times 10^{21}$ atoms cm$^{-2}$), which correlates quite well with the X-ray results. The quantity of absorbing gas in the Galaxy along the line of sight to the LMC sets the minimum column density we should expect to see. This is $(5\text{–}6) \times 10^{20}$ atoms cm$^{-2}$, which appears to be consistent with the columns derived for DEM 71, N23, and perhaps 0453−68.5.

The reader will notice that both the fitted shock temperature and ionization timescale are consistently higher for the Coulomb equilibration timescales model compared to the full equilibration one, as a direct consequence of the lag of the electron temperature with respect to the ion temperature in the former case. However, the difference in temperature is small, $\lesssim 30\%$, and is comparable to the statistical uncertainty in the parameters. The ionization timescale differs by a much larger amount, up to factors of $\sim 3$, the consequences of which we discuss below when we compare the ionization and dynamical ages. The other fitted parameters, i.e., column density, normalization and the elemental abundances, also agree to within the statistical errors. We note that the quality of the fits as indicated by the reduced $\chi^2$ values is nearly the same under the two different assumptions we have made about electron-ion equilibration timescales, which is unfortunate since it means that our study can not use this to discriminate between the two cases.

From the fitted normalization of the X-ray spectra ($N$) and shock temperature ($T_s$), we estimate the ISM number density of hydrogen ($n_0$), the Sedov dynamical age ($t_d$), the initial explosion energy ($E_0$), and the swept-up mass ($M_{SU}$), using the following equations:

$$n_0 = 13\left(\frac{N}{10^{12}\ \mathrm{cm}^{-5}}\right)^{1/2}\left(\frac{\theta_R}{10''}\right)^{-3/2}\left(\frac{D}{50\ \mathrm{kpc}}\right)^{-1/2} \times \left(\frac{\Omega}{4\pi}\right)^{-1/2} \mathrm{H\ cm}^{-3}\,, \quad (1)$$

$$t_d = 10^3\left(\frac{kT_s}{1\ \mathrm{keV}}\right)^{-1/2}\left(\frac{\theta_R}{10''}\right)\left(\frac{D}{50\ \mathrm{kpc}}\right)\mathrm{yr}\,, \quad (2)$$

$$E_0 = 0.33 \times 10^{51}\left(\frac{kT_s}{1\ \mathrm{keV}}\right)\left(\frac{N}{10^{12}\ \mathrm{cm}^{-5}}\right)^{1/2}\left(\frac{\theta_R}{10''}\right)^{3/2} \times \left(\frac{D}{50\ \mathrm{kpc}}\right)^{5/2}\left(\frac{\Omega}{4\pi}\right)^{-1/2}\ \mathrm{ergs}\ , \quad (3)$$

$$M_{\mathrm{SU}} = 26\left(\frac{N}{10^{12}\ \mathrm{cm}^{-5}}\right)^{1/2}\left(\frac{\theta_R}{10''}\right)^{3/2}\left(\frac{D}{50\ \mathrm{kpc}}\right)^{5/2} \times \left(\frac{\Omega}{4\pi}\right)^{1/2} M_\odot\ , \quad (4)$$

where $\Omega$ is the solid angle subtended by the remnant shell with respect to the remnant center and is a factor that is intended to take account of possible incompleteness of the spherical structure. Spherical symmetry ($\Omega = 4\pi$) was assumed in order to compute the values of the derived quantities given in Table 2. The physical radii in Table 2 are based on the angular X-ray size from Mathewson et al. (1983) and our assumed distance of 50 kpc to the LMC. In calculating the swept-up mass we assumed that the mean ionic weight was $1.4m_{\mathrm{H}}$.

Figure 2 plots the ambient ISM hydrogen number density and derived explosion energy versus radius for the several remnants. The ambient density is uncorrelated with remnant size for our sample. There are some potential biases that work against finding SNRs in the upper right-hand corner of this figure (radiative cooling) or the lower left-hand corner (rapid expansion), but given the lack of a statistically significant correlation, these issues are moot.

The range of derived $E_0$ values varies over an order of magnitude from a high of $6 \times 10^{51}$ ergs for N132D to a low of $5 \times 10^{50}$ ergs for N23. Recall that $E_0$ depends on $\Omega^{-1/2}$ and that we assumed the maximum value for $\Omega$ ($=4\pi$; i.e., spherical symmetry), so the explosion energies we quote are in some sense lower bounds. In particular, N23, which has the lowest derived $E_0$ value, also is the remnant that has the most asymmetric X-ray image. Uncertainty in the distance to individual SNRs owing to the thickness of the LMC, for example, is probably not much more than 10%, which translates to a $\sim$25% error in $E_0$. As for the ambient density, we find no statistically significant evidence for a dependence of the derived explosion energy on remnant size. This is in contrast to optical studies of LMC SNRs (Dopita 1979; Danziger & Leibowitz 1985) that have claimed a rather strong dependence of $E_0$ on remnant size, even for some of the same remnants as in our sample. These results were never particularly convincing (at least to us) since they were based on extrapolating the pressure behind the shock, as estimated from the density-sensitive [S II] lines, to estimate the energy density in the interior of the entire remnant. Blair, Kirshner, & Chevalier (1981) have pointed out that the apparent relation between $E_0$ and radius could be explained if the [S II]–emitting regions are dominated by magnetic pressure, rather than thermal pressure as assumed otherwise. Our explosion energy values are based on the well-constrained observables of shock temperature, radius, and emission measure and rely on the applicability of the Sedov evolutionary model. Whether or not this is justified is the next issue we consider.

One of the assumptions of Sedov-phase remnant models is that they are adiabatic, or energy conserving, which implies that radiative cooling is insignificant. Cox (1972) identified a number of evolutionary phases in the life of an SNR as it makes the transition from an adiabatic remnant to a fully radiative one. In his picture, the onset of radiative cooling occurs when the temperature distribution begins to deviate from the adiabatic model (temperature sag phase) at an age given by

$$t_{\mathrm{sag}} = 1.33 \times 10^4\left(\frac{E_0}{10^{51}\ \mathrm{ergs}}\right)^{2/11} \times \left(\frac{\Lambda}{10^{-22}\ \mathrm{ergs\ cm^3\ s^{-1}}}\right)^{-5/11}\left(\frac{n_0}{1\ \mathrm{cm}^{-3}}\right)^{-7/11}\ \mathrm{yr}\ , \quad (5)$$

where the cooling coefficient $\Lambda$ is of order $10^{-22}$ ergs cm$^3$ s$^{-1}$. Using $E_0$ and $n_0$ from Table 2, $t_{\mathrm{sag}}$ varies from $7 \times 10^3$ yr for N63A to $3 \times 10^4$ yr for 0453−68.5. For all the remnants in our sample, $t_{\mathrm{sag}}$ is at least 50% larger than the dynamical age quoted in Table 2, which shows that, at least from this point of view, the Sedov model is justified.

As we mentioned in § 3.2, we can estimate the ionization age ($t_i$) of our remnant sample from the fitted $n_0\, t_i$ values by

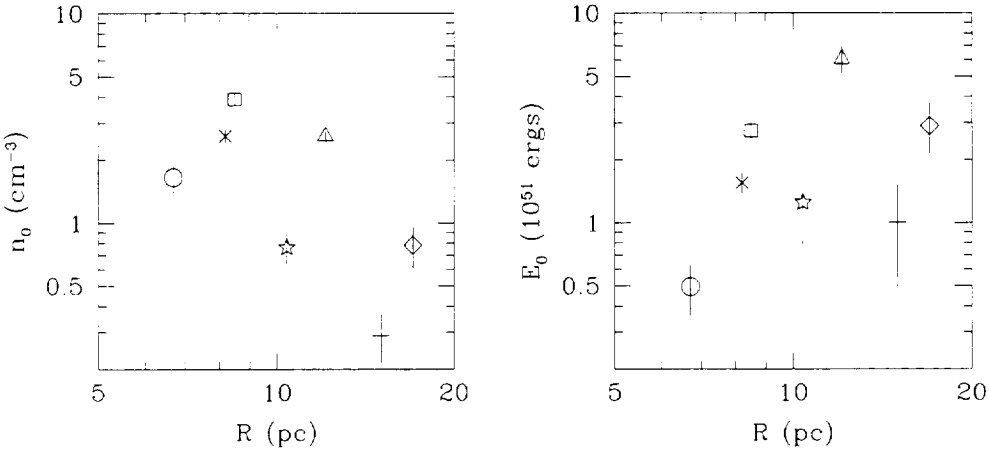


FIG. 2.—Ambient ISM hydrogen number density vs. remnant radius (*left-hand panel*) and initial supernova explosion energy vs. radius (*right-hand panel*). Values for all seven remnants are shown using different symbols: the circle, cross, square, star, triangle, plus sign, and diamond correspond to N23, N49, N63A, DEM 71, N132D, 0453−68.5, and N49B, respectively. Error bars include only the statistical uncertainty (at the 90% confidence level) from fits for temperature and emission measure. Results plotted are the average of the values obtained under the two different model assumptions about the timescale for electron-ion temperature equilibration.

employing the $n_0$ value derived from the emission measure (eq. [1]). Because of the difference in fitted ionization timescales between the full and Coulomb temperature equilibration models, there is a significant difference in the inferred ionization ages as well. In Figure 3 we plot the correlation between ionization age (for both models) and dynamical age. For all remnants, the full equilibration model predicts an ionization age that is considerably lower than the dynamical age with differences ranging from $\sim 1.3$ $\sigma$ (for 0453−68.5) to $\sim 9$ $\sigma$ (for N49B). On the other hand, under the assumption of Coulomb equilibration timescales, there is excellent agreement (a difference of $\lesssim 1.2$ $\sigma$) between the ionization and dynamical ages for N23, N49, DEM 71, and 0453−68.5, although the ionization ages of N132D, N63A, and N49B all continue to remain low. This discrepancy for the latter three remnants cannot be resolved by invoking clumping of the X-ray–emitting gas, since that would increase our estimate for $n_0$ and consequently lower the inferred ionization ages even further. Similarly, reducing $\Omega$ from its spherically symmetric value of $4\pi$ would also result in reduction of the ionization ages as well. We believe that the most likely reason for the discrepancy is that the Sedov model has overestimated the dynamical ages of these remnants.

In this case, it is not coincidental that the three remnants with significant differences between their ionization and dynamical ages are also the remnants with unusually high inferred values of initial SN explosion energy: $\gtrsim 3 \times 10^{51}$ ergs. A plausible explanation for both discrepancies is that these remnants exploded within preexisiting low-density cavities in the ISM. The low interior density allows the SN blast wave to propagate rapidly to the cavity wall, where it then encounters denser gas, begins to slow down, and emits copious amounts of X-rays. This scenario naturally results in a reduction of both the dynamical age and the initial explosion energy from that inferred assuming the Sedov model. Note that Hughes (1987) proposed precisely this same model to account for the difference between the Sedov dynamical age and the kinematic age determined from the expansion of high-velocity oxygen-rich filaments in N132D (more on this in § 7.5 below). It is encouraging that our independent estimate of N132D's age based on its ionization timescale confirms this earlier result, and it gives us confidence in the identification of N63A and N49B as two more examples of this phenomenon in the LMC. This turns out to be extremely important, since it allows us to identify these three remnants as the core-collapse supernovae of massive stars whose strong stellar winds modified the surrounding ISM.

The four other SNRs, N23, N49, DEM 71, and 0453−68.5, are fully consistent with the Sedov model under the assumption that the electrons and ions do not attain the same temperature at the shock front but, rather, exchange energy slowly through Coulomb collisions. This hypothesis appears to be supported by other observations of SNRs; perhaps the best evidence to date comes from the remnant of SN 1006 in the Galaxy. Based on comparing shock models to the observed far-UV emission lines of the

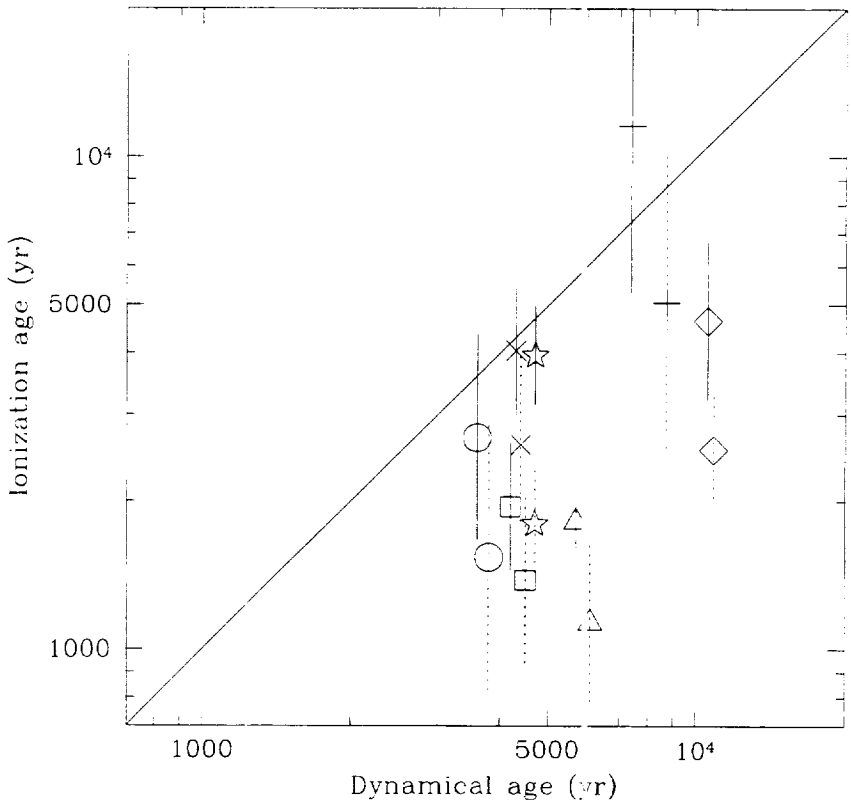


FIG. 3.—Remnant age determined from the fitted ionization timescale vs. the dynamical age derived from the Sedov solution. The different symbol types refer to the different remnants (circle, cross, square, star, triangle, plus sign, and diamond correspond to N23, N49, N63A, DEM 71, N132D, 0453−68.5, and N49B, respectively). Error bars include only the statistical uncertainty from fits for the ionization timescale. Data points with dotted error bars (at the 90% confidence level) are from the results assuming full electron-ion temperature equilibration at the SNR shock front, while the solid error bars refer to results using Coulomb equilibration timescales.

remnant, Laming et al. (1996) find that the electrons at the shock front in SN 1006 can attain a temperature of no more than ~20% of the ion temperature and that even lower equilibration values are preferred by their data. This is the strongest observational evidence in the literature against full electron-ion equilibration at SN shock fronts. We close this section by noting that the consistency of these four SNRs with the Sedov model appears to extend even to the value we find for their average initial explosion energy $E_0 = (1.1 \pm 0.5) \times 10^{51}$ ergs, where the uncertainty comes from the rms object-to-object scatter.

## 5. ABUNDANCES

### 5.1. *Correlations*

Figure 4 displays the complete set of abundance results for the seven LMC remnants, where we have chosen to average the fitted abundances (and errors) that come from our two different assumptions about the timescale for electron-ion temperature equilibration. Overall, we find abundances that are less than cosmic by factors of 2–5, as expected for interstellar gas in the LMC. At first glance the different remnants yield rather similar abundances for the same elemental species, but a closer look reveals some notable exceptions that we discuss further below.

In order to check for systematic effects that might have biased the fitted abundances, we carried out the following correlation analysis. First we determined the mean metallicity for each remnant by calculating the error-weighted average of the fitted abundance values (presented in the bottom half of Table 2), including both sets of values from the full and Coulomb equilibration models. We searched for correlations between these mean metallicities and the various fitted or derived parameters using the Spearman rank-order test. The correlation coefficients ($r_s$) for mean metallicity versus $N_H$, $T_s$, $n_0 t_i$, and $N_s$ are $-0.14$, 0.04, 0.61, and 0.21, respectively, although none of the correlations were statistically significant (among these the highest significance was ~93% for metallicity versus $n_0 t_i$). This is very encouraging since it shows that there are no obvious systematic biases in the derived abundances that are directly linked to the spectral fits. Likewise there are no statistically significant correlations between mean metallicity and any of the derived parameters $E_0$, $n_0$, and $M_{SU}$. There are, however, two statistically significant correlations: mean metallicity versus age ($r_s = -0.89$, significance ~99.6%) and mean metallicity versus radius ($r_s = -0.96$, significance ~99.97%). Plots of these latter two correlations, plus the correlation of metallicity versus swept-up mass, are shown in Figure 5. The error bars displayed are estimates based on the weighted rms scatter from the individual abundance measurements of the six species considered.

The correlation in the left-hand panel of Figure 5 shows that the smaller remnants are somewhat enhanced in metallicity with respect to the larger ones. In fact, this correlation also holds when the elemental species are considered individually. Specifically, the oxygen, neon, silicon, and iron abundances show correlations with radius that are significant at the 99.97%, 94%, 96% and 95% confidence levels, respectively, while the magnesium and sulfur abundances are essentially uncorrelated with remnant size. Note that these correlations can be seen in Figure 4 since the data points corresponding to the individual remnants are plotted for each species from left to right in order of remnant size.

H II regions in the LMC are known to show a significant correlation between distance from the galaxy center and their oxygen abundance based on measurements of [O II] and [O III] from warm photoioinized gas. The abundance gradient has a value of $-0.048 \pm 0.019$ dex kpc$^{-1}$ (Kobulnicky 1997). We determined the deprojected radial distances of our remnants from the center of the LMC assuming a flat disk geometry, an inclination angle of 27°

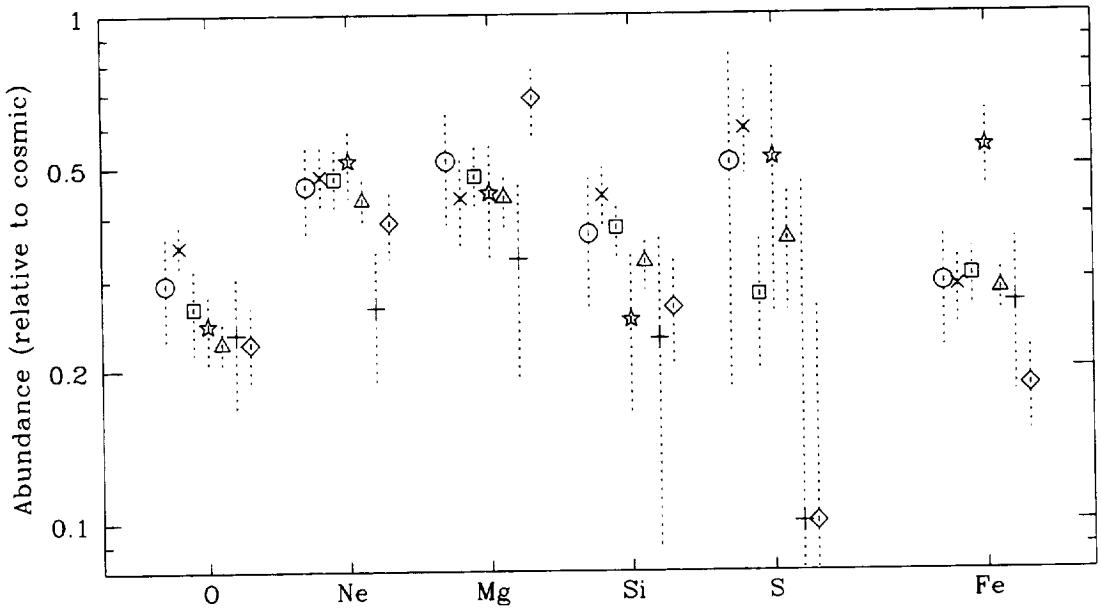


FIG. 4.—Elemental abundances relative to the cosmic values derived from *ASCA* X-ray spectroscopy of LMC SNRs. Values for all seven remnants are shown using different symbols: the circle, cross, square, star, triangle, plus sign, and diamond correspond to N23, N49, N63A, DEM 71, N132D, 0453−68.5, and N49B, respectively. Error bars include only the statistical uncertainty (at the 90% confidence level) from the spectral fits. Results plotted are the average of the values obtained under the two different model assumptions about the timescale for electron-ion temperature equilibration. We can determine only upper limits to the S abundances of 0453−68.5 and N49B. These points are plotted at a value of 0.1, and the upper limit lies at the top of the error bar.

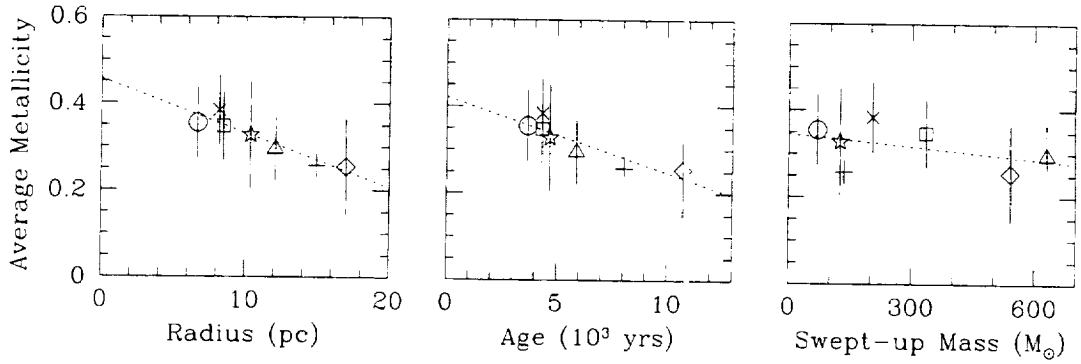


FIG. 5.—Mean metallicity (relative to cosmic values) vs. radius (*left-hand panel*), dynamical age derived from the Sedov solution (*middle panel*), and swept-up mass (*right-hand panel*). The different symbol types refer to the different remnants (circle, cross, square, star, triangle, plus sign, and diamond correspond to N23, N49, N63A, DEM 71, N132D, 0453−68.5, and N49B, respectively). Error bars represent the rms scatter in the individual fitted abundances of the various elemental species considered. Results plotted are the average of the values obtained under the two different model assumptions about the timescale for electron-ion temperature equilibration. The only significant correlations are between metallicity and either radius or age.

between the normal to the disk and the line of sight, position angle of 165°, and center at $5^h24^m$, −69°48′. The remnants in our sample cover galactocentric radial distances from 0.3 to 3.3 kpc, which would suggest a 30% difference in abundance based on the H II regions. In fact, the mean metallicity is uncorrelated with distance from the center of the LMC, and our data are best described by a model with no gradient in chemical abundance with galactocentric distance.

The interpretation we favor is that the metallicity-radius correlation indicates the presence of newly produced SN ejecta in at least some of the remnants of the sample. This is not particularly surprising, since we know that small, young Galactic remnants such as Tycho and Cas A show very strong and prominent X-ray emission from supernova ejecta, while larger ones, like the Cygnus Loop and Vela, do not. Furthermore, earlier work by us (Hughes et al. 1995) on the *ASCA* X-ray spectra of the three LMC SNRs N103B, 0509−67.5, and 0519−69.0 (with radii between 3 and 4 pc) revealed them to be dominated by ejecta. It is perhaps a little surprising that the correlation is so good with radius or age but not with swept-up mass. Apropos of this point is the observation that the only remnant of these seven previously known to contain newly minted SN ejecta is N132D, which has the largest swept-up mass in our sample! Clearly the fate of the metals ejected by a SN is complex, which makes prediction of their emission properties as a function of time rather difficult. Such a study is beyond the scope of our work here, and we direct the interested reader to Tenorio-Tagle (1996), where a discussion of some of the relevant issues for Type II supernovae is given.

Figure 5 puts the level of enrichment (i.e., the difference between the average metallicity of the smaller SNRs compared to the larger ones) at a value of ~0.1. Interestingly, this difference is comparable to the amount of metals that models predict should be produced and ejected by certain mass ranges of progenitor stars. For example if we take the nucleosynthetic yields for a progenitor with a main-sequence mass of 13 $M_\odot$ from Thielemann, Nomoto, & Hashimoto (1996) and dilute it with 200 $M_\odot$ of swept-up material (the median value in our sample), then the fractional abundances of O, Ne, and Mg would increase by ~0.1. In the same way the abundances of Si, S, and Fe would increase by an amount equal to ~0.4. The nucleosynthetic yields of the lighter elements, in particular, are a strong function of main-sequence mass, and, thus, diluting the ejecta from a 25 $M_\odot$ progenitor with 200 $M_\odot$ of ISM would result in the O abundance increasing by ~1. The preceding points are intended to indicate the order-of-magnitude agreement between the amount of enrichment we actually see in the LMC SNR sample and the amount that might be expected in the very simplest scenario imaginable for the mixing of ejecta and ISM in SNRs.

In addition to this statistical evidence for ejecta enrichment, there is direct evidence as well. In particular, we refer the reader to Figure 4, where the anomalously high iron abundance for DEM 71 can be clearly seen. Although some other individual abundances are slightly discrepant with respect to their neighbors (e.g., the magnesium abundance for N49B), only the case of the iron abundance of DEM 71 is statistically significant. This will be discussed in more detail below (§ 7.4).

### 5.2. *Depleted Abundances?*

Another question concerning our abundance measurements that must be addressed is the possible depletion of metals onto dust grains in the interstellar medium. Interstellar gas is believed to be significantly depleted in magnesium, silicon, calcium, and iron (with abundances roughly an order of magnitude less than solar) but only slightly depleted in oxygen and sulfur. Depletions depend on the mean gas density of the environment, in general, growing larger with increasing gas density (Mathis 1990). An important constraint is that neon and argon, as inert, noble gases, are not expected to form grains and thus should not be depleted in the gas phase. Our abundance results appear to be in conflict with this picture of the dusty ISM. In fact, the abundance we find for neon is essentially the same as that of magnesium, silicon, and sulfur, while oxygen and iron are no more than about a factor of two less.

Vancura et al. (1994) study the effects of interstellar grains on the predicted X-ray and IR emission of supernova shock waves and find that the X-ray spectra of SNRs are substantially influenced by the gradual destruction of dust grains, primarily through collisions with protons and He nuclei, in the postshock flow. Their models are based on a planar shock geometry and do not include the deceleration of the blast wave, so their results are not directly applicable to our measurements. Nevertheless, with this as a warning we attempt a comparison. The fraction of initial mass remaining in grains is a strong function of the swept-up column density behind the shock. As an estimate of the swept-up

column for our remnants, we use the quantity $n_0 R/6$, which simply assumes that the entire mass of shocked gas in the SNR is contained in a uniform density shell of thickness $R/12$ and takes the average value of the swept-up column at the inner and outer edges of the shell. The smallest value of this quantity among the remnants in our sample is $2.3 \times 10^{18}$ cm$^{-2}$ (for 0453−68.5), while the largest is $1.7 \times 10^{19}$ cm$^{-2}$ (for N63A). According to Figure 3 in Vancura et al. (1994), the fraction of initial mass that should have remained in grains is 60% for our minimum swept-up column and 20% for the maximum one. For the species magnesium, silicon, and iron, which are supposed to be nearly entirely depleted in the gas phase, then the mean abundances should vary by about a factor of 2.4 over this range in swept-up column. We just do not see such large variations in the abundances of these elements as a function of swept-up column density. Furthermore, there is not even a significant correlation between swept-up column and abundance for magnesium and iron, although the correlation for the silicon abundance versus swept-up column density is significant at the 97.4% confidence level. Weighing all the evidence presented in this and the preceding paragraph leads us to conclude that we have not detected evidence for the destruction of swept-up interstellar dust grains on the expected timescales in these LMC SNRs. This suggests that either the gas phase of the ISM is not significantly depleted in metals or the timescale for the destruction of dust grains behind SN shock waves is shorter than previously thought.

### 5.3. *Metal Abundances of the LMC*

We determine the gas-phase abundances of the LMC by averaging, for each elemental species, the fitted abundances from the seven remnants. As before, we include both sets of values corresponding to the full and Coulomb equilibration models. The uncertainties quoted come from the weighted rms scatter among the 14 measurements. For sulfur, the values from 0453−68.5 and N49B are not included, since these SNRs provided only upper limits. Table 3 lists the average abundances and uncertainties expressed as [M/H] = 12 + log (M/H), and Figure 6 plots the abundances, relative to the cosmic values we assumed, versus elemental species.

The third column of Table 3 lists the LMC chemical abundances of oxygen, neon, and sulfur determined from UV/optical spectra of H II regions as summarized in a review by Dufour (1984). The agreement between the X-ray SNRs and H II regions for the different elements is impressive. More recently, RD92 presented the results of a large study to establish a consistent set of global abundances for the Large and Small Magellanic Clouds covering the elements from $Z = 2$ to $Z = 63$. This work was based on spectral analyses of F supergiants for the abundances of the heavier elements (e.g., Mg, Si, and elements with $Z > 18$) (Russell & Bessell 1989) and the modeling of spectra from H II regions and SNRs for the lower $Z$ elements (e.g., He, O, Ne, and S) (Russell & Dopita 1990). Our values and those from RD92 are also in general agreement with the possible exception of magnesium and silicon, where the RD92 values appear anomalously high compared to the other species, although it should be noted that the abundance of silicon was quoted in RD92 as being highly uncertain. It is now clear that these species are not anomalously abundant in the ISM of the LMC compared to, say, neon and sulfur. Thus the results from X-ray SNRs have proved to be especially valuable in filling this important gap in our knowledge of the abundances of the intermediate-mass elements and in providing a set of accurate abundance values determined in a consistent manner for elemental species over a broad range of atomic number.

Now we would like to address the reliability of our abundance estimates. The abundances of neon, magnesium,

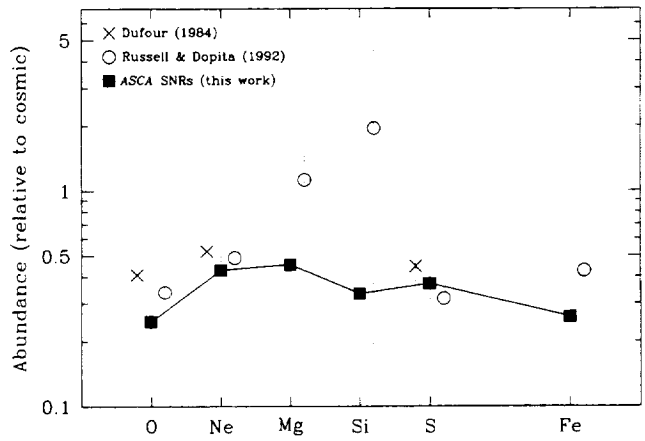


FIG. 6.—Average chemical abundances of the LMC relative to the cosmic values plotted as a function of elemental species. The gas-phase abundances of the LMC derived from optical and UV studies of H II regions are shown as the crosses (Dufour 1984). More recent results from Russell & Dopita (1992), shown as the circles, are based on detailed modeling of optical/UV spectra from H II regions, SNRs, and supergiant stars. The silicon abundance in Russell & Dopita's work is highly uncertain as indicated by our use of a large error bar for this species. The filled squares, showing our results from *ASCA* X-ray spectroscopy of SNRs, are in excellent agreement with the values derived from longer wavelength observations.

TABLE 3

LMC ABUNDANCES[a]

| Species | *ASCA* X-Ray SNRs[b] | H II Regions[c] | H II Regions, SNRs, Supergiant Stars[d] |
|---|---|---|---|
| [O/H] ..... | 8.21 ± 0.07 | 8.43 ± 0.08 | 8.35 ± 0.06 |
| [Ne/H] ..... | 7.55 ± 0.08 | 7.64 ± 0.10 | 7.61 ± 0.05 |
| [Mg/H]..... | 7.08 ± 0.07 | ... | 7.47 ± 0.13 |
| [Si/H] ..... | 7.04 ± 0.08 | ... | 7.81[e] |
| [S/H] ..... | 6.77 ± 0.13 | 6.85 ± 0.11 | 6.70 ± 0.09 |
| [Fe/H]..... | 7.01 ± 0.11 | ... | 7.23 ± 0.14 |

[a] Expressed as [M/H] ≡ 12 + log(M/H).
[b] This work, errors are the rms variation among the seven SNRs.
[c] Dufour 1984.
[d] Russell & Dopita 1992.
[e] Highly uncertain.

TABLE 4

UPPER LIMITS TO POWER-LAW X-RAY EMISSION

| SNR | Energy Band Fitted (keV) | 3 $\sigma$ Upper Limit $L_X$ (0.2–4 keV) ($10^{35}$ ergs $s^{-1}$) |
|---|---|---|
| N23 | 3–10 | 2.6 |
| N49 | 4–10 | 7.6 |
| N63A | 4–10 | 13.5 |
| DEM 71 | 3–10 | 5.1 |
| N132D | 4–10 | 22.4 |
| 0453−68.5 | 3–10 | 2.3 |
| N49B | 3–10 | 1.9 |

silicon, and sulfur that we derive from the *ASCA* X-ray spectra of SNRs are least subject to systematic uncertainty since they come from fits to K-shell emission lines of well-understood helium-like and hydrogen-like ionic species. Our iron abundance is based on the L-shell blend at $\sim 1$ keV, so there is some systematic uncertainty owing to inadequate or poorly known atomic physics and the incompleteness of the line lists used in the spectral models. Our oxygen abundance is also somewhat less reliable because the oxygen K-shell lines are near the low-energy cutoff of the SIS detectors where the efficiency is low and the calibration is less certain. Furthermore, of all the species considered, the oxygen abundance is most sensitive to the precise variation of temperature and ionization through the interior of our Sedov models. For example, over the outer 10% radius of the Sedov models (from which nearly all of the X-ray emission comes), the ionization fraction of O VIII (hydrogen-like) varies by more than an order of magnitude (decreasing from the edge in toward the center). By contrast, Si XIV (also hydrogen-like) is the dominant ionic species and varies by less than a factor of 2 over the same radial range. Thus, our models predict that the oxygen emission should be coming from a narrow shell near the edge of the SNR, while the silicon emission should be distributed over a larger radial extent. Future higher spatial resolution X-ray observations with *AXAF* will be able to measure these variations and thereby provide more accurate abundance results that are less dependent on the model details. However, the comparison between our results and previous ones shown in Figure 6 suggests that the systematic error in the oxygen and iron abundances derived from our work is not much more than $\sim 0.1$–0.2, with our values being slightly lower than the optical/UV ones.

## 6. LIMITS ON HIGH-ENERGY X-RAY EMISSION

X-ray imaging at energies above $\sim 4$ keV has been one of the most important recent developments in the search for pulsar-powered synchrotron nebulae (PSNs) in supernova remnants. Studies with *ASCA* in the past 2 yr have confirmed the existence of, or directly detected, PSNs in several Galactic SNRs including Kes 73 (Blanton & Helfand 1996), G11.2−0.3 (Vasisht et al. 1996), W44 (Harrus, Hughes, & Helfand 1996), CTA-1 (Slane et al. 1997), and MSH 11-62 (Harrus, Hughes, & Slane 1998). The reason for this is simple: above 4 keV thermal emission from shock-heated gas is negligible, while hard power-law emission from a PSN remains relatively strong. The discovery of a PSN in a supernova remnant is pivotal, since it conclusively establishes the remnant as the product of a massive-star core-collapse SN. The only LMC SNRs that can, without question, be put in this class are the SNRs 0540−69.3 and N157B, both of which contain rapidly rotating pulsars with periods of 50.3 ms (Seward, Harnden, & Helfand 1984) and 16.1 ms (Marshall et al. 1998), respectively, and whose X-ray emissions are dominated by the nonthermal power law from the PSN. Because of the known distance to the LMC, these PSNs have well-determined soft (0.15–4.5 keV) X-ray luminosities of $9.5 \times 10^{36}$ ergs $s^{-1}$ (0540−69.3) and $2.5 \times 10^{36}$ ergs $s^{-1}$ (N157B).

A factor of $>2500$ separates the luminosity of 0540−69.3 from that of the faintest known Galactic PSN that surrounds PSR B1853+01 in W44. It is quite possible that PSNs with luminosities in this range are present in some of the LMC SNRs in our sample even though all are clearly dominated by thermal emission. However, the arcminute imaging capability of *ASCA*, which is adequate for spatially resolving thermal and nonthermal emission in Galactic SNRs, is insufficient for doing so for LMC SNRs, where a 2 pc diameter PSN would subtend merely 8″. Thus any information on PSN from *ASCA* will have to come from the integrated spectra of individual LMC remnants. At this time we do not claim unambiguous detection of nonthermal X-ray emission for any of the seven SNRs in this study because the SIS emission observed above $\sim 3$ keV is comparable to the fluctuations in background.

In order to set quantitative limits, we fitted the high-energy portion of the SIS spectra to a power-law model ($dN/dE \sim E^{-\alpha_p}$) with a fixed photon index of $\alpha_p = 2.0$. For the four fainter SNRs (N23, DEM 71, 0453−68.5, and N49B) the band fitted was 3–10 keV, while for the brighter ones (N49, N63A, and N132D) we used the 4–10 keV band. Acceptable fits were obtained in all cases. The 3 $\sigma$ upper limits to the flux of this component were then used to calculate unabsorbed luminosities in the soft X-ray band as shown in Table 4.

These luminosity values are in the range expected for PSNs (Seward & Wang 1988). The high limit for N63A is rather interesting since this is one of the remnants, along with N132D and N49B, that is likely to have arisen from a core-collapse supernova and therefore might be expected to contain a PSN. Note that the high upper limit value for N132D largely reflects the short *ASCA* exposure on the remnant. The limits we set for the others are consistent with them *not* containing high-luminosity PSNs powered by rapidly spinning young pulsars, in agreement with our age estimates for them assuming Sedov evolution.

Current theories predict that SNe Ia should not produce pulsars, so their remnants should not contain PSNs. It is possible that these SNRs may show nonthermal X-ray emission from electrons accelerated to high energies at the shock front by the first-order Fermi process as observed in SN 1006 (Koyama et al. 1995). This emission tends to be steeper spectrum ($\alpha_p = -2.4$ to $-3$) and fainter (SN 1006's soft $L_X$ is $\sim 4 \times 10^{34}$ ergs $s^{-1}$) than that of PSNs and therefore much more difficult to detect in LMC SNRs. The upper limit to the high-energy luminosity for DEM 71, which is the only securely identified remnant of a SN Ia in the sample, is about an order of magnitude higher than SN 1006's luminosity.

## 7. COMMENTS ON INDIVIDUAL REMNANTS

### 7.1. *N23*

N23 is not a particularly well studied remnant. Chu & Kennicutt (1988; hereafter CK88) tentatively classify it as

the remnant of a massive star SN (Population I) based on the high density of OB stars nearby and its proximity to a modest molecular cloud (Cohen et al. 1988). Recently Banas et al. (1997) searched for CO emission on smaller spatial scales ($\sim 20''$) than the Cohen survey but found nothing significant that could be associated with the remnant. We note that N23 has one of the lowest column densities in the sample (a factor of 3–4 less than N49 and N49B), which may make direct association with a molecular cloud unlikely. As the smallest remnant in our sample, N23 is an important object that supports the statistical evidence for SN ejecta enrichment discussed above.

### 7.2. *N49*

Images of N49 in the optical, X-ray, and radio bands (Vancura et al. 1992; Dickel et al. 1995) are in general agreement as far as the broad picture of its morphology is concerned. The remnant is brightest in the southeast and trails off in brightness toward the northwest. On smaller scales, however, individual features differ in relative brightness across the electromagnetic spectrum. The asymmetry and high X-ray and optical flux are due to the enhanced ambient density toward the southeast, where a moderate-sized molecular cloud sits (Banas et al. 1997). The large X-ray–absorbing column density that we derive further indicates a high-density environment. This is also true of the mean optical reddening of N49, $E(B-V) \sim 0.37$ (Vancura et al. 1992), which is quite a bit more than the reddening due to the Galaxy, $E(B-V) \sim 0.07$ (Fitzpatrick 1985). We note that the X-ray–absorbing column density and interstellar reddening toward N49 are in excellent agreement with the ratio of these quantities, $N_{\rm H}/E(B-V) = (6.8 \pm 1.6) \times 10^{21}$ atoms cm$^{-2}$ mag$^{-1}$, given by Ryter, Cesarsky, & Audouze (1975).

By comparing shock models to their optical and UV spectra of N49, Vancura et al. (1992) estimate the abundances of several species. For oxygen and sulfur, their abundances are some 50% higher than ours, while their iron abundance is in numerical agreement with ours. The other species in common (neon, magnesium, and silicon) agree to within a factor of 2, but the optical results are based on lines from only a single ion and are therefore potentially less reliable. Since Vancura et al. (1992) quote no abundance uncertainties, it is difficult to assess the significance of these differences.

Vancura et al. (1992) also develop a self-consistent scenario for the evolution of N49. Optical emission comes from slow shocks (velocity range of 40–270 km s$^{-1}$) driven into dense clouds (20–940 cm$^{-3}$) distributed in thin sheets that are located at places where the SN blast wave is interacting with the nearby molecular cloud. X-ray emission comes from a fast shock (730 km s$^{-1}$) propagating through the intercloud medium (preshock density of 0.90 cm$^{-3}$). They derive a Sedov age of roughly 5400 yr by assuming an explosion energy of $10^{51}$ ergs. In this picture the prevailing ISM was largely unaffected by the progenitor star, in direct contrast to the view espoused by Shull et al. (1985), where the SN blast wave is interacting with the dense shell of the progenitor star's Strömgen sphere.

Our results show that the X-ray data on N49 are consistent with Sedov evolution in two ways. First, the initial SN explosion energy we derive from our fitted shock temperature is consistent with the canonical value of $10^{51}$ ergs. Second, the two ages we determine for the remnant, i.e., the ionization age and the Sedov dynamical age, are entirely consistent with each other. Thus the X-ray, optical, and UV data all tend to support the Vancura et al. (1992) picture for the evolution of N49, while they tend not to favor the Shull et al. model of an explosion within a preexisting cavity in the ISM.

There is at least one other interesting aspect of N49, namely that it is positionally coincident with the 1979 March 5 $\gamma$-ray burst event, one of only three known soft $\gamma$-ray repeaters (SGRs). Rothschild, Kulkarni, & Lingenfelter (1994) claim that the burst position of SGR 0525−66 is coincident with an unresolved source at the northern edge of N49, based on soft X-ray images from the *ROSAT* high-resolution imager (HRI). Our *ASCA* results do not preclude the possibility that this source has a hard power-law spectrum. In fact, the upper limit we derive for the power-law emission from N49 (Table 4) corresponds to an HRI count rate of 0.022 s$^{-1}$, which is greater than the actual count rate, $0.0151 \pm 0.0013$ s$^{-1}$, of the unresolved source in the HRI image. In addition, our upper limit to the hard power-law emission implies a luminosity $< 4 \times 10^{35}$ ergs s$^{-1}$ (2–10 keV band), which is comparable to the persistent X-ray luminosity of AX 1805.7−2025 ($3 \times 10^{35}$ ergs s$^{-1}$; Murakami et al. 1994). This source is the counterpart to one of the other SGRs (SGR 1806−20) and is believed to be an isolated neutron star powering a radio nebula in the SNR G10.0−0.3 (Kulkarni et al. 1994). Getting back to N49, Dickel et al. (1995) claim to have found no evidence for a radio or optical counterpart to SGR 0525−66. They do note that a compact radio feature lies near the quoted position of the unresolved X-ray source, but they dismiss it as being unrelated largely owing to a 5″ difference in the radio and X-ray positions. However, this conclusion may be premature, since a few arcseconds is roughly the accuracy for absolute position determination by *ROSAT*. It is probably fair to say that the issue of the counterpart to SGR 0525−66 has not been completely resolved and awaits further study with *AXAF*.

### 7.3. *N63A*

N63A is the second brightest X-ray–emitting SNR in the LMC, and its derived shock temperature, ambient density, and abundances (Table 2) turn out to be very similar to those of the other bright LMC SNRs, N49 and N132D. However, unlike both N49 and N132D, N63A's morphology varies quite a bit across the electromagnetic spectrum. At optical wavelengths, the remnant consists of three bright lobes of emission embedded in the extended diffuse H II region N63. Two of the three lobes consist of shock-heated gas, while the third is a photoionized region. The shock-heated gas appears to be of normal composition for the LMC and is expanding at moderate velocities, $\sim 250$ km s$^{-1}$ (Shull 1983). In the radio band N63A shows a thick asymmetric shell-like structure $\sim 65''$ in diameter with enhancements at the positions of the bright optical features (Dickel et al. 1993). The X-ray image (Mathewson et al. 1983) also displays a thick shell of roughly the same size as the radio one but without any obvious enhancements corresponding to features at the other wavelengths. Curiously, the bright optical region is only about one-third the size of the X-ray or radio shells and is displaced westward by about 15″ from their respective centers.

Based on its location in an H II region, as well as its positional coincidence with the OB association NGC 2030,

it is not surprising that this remnant is considered to have had a Population I progenitor (CK88). This could also be consistent with our suggestion that N63A exploded within a wind-blown cavity in the ISM. We derive the highest ambient ISM density for this remnant, nearly 4 $cm^{-3}$, yet other signs of such a high-density environment are not obvious. For example, unlike both N49 and N132D, there is no evidence for molecular emission near N63A from either the Columbia survey of the LMC (Cohen et al. 1988) or from higher angular resolution SEST data (Israel et al. 1993). It is clear that a lot more work will be needed before we obtain a comprehensive picture of this enigmatic SNR and its environment.

### 7.4. *DEM 71*

There is a class of SNRs that show only hydrogen lines in their optical spectra with virtually no emission from collisionally excited forbidden lines, e.g., [O III] and [S II], as usually seen from SNRs. Tycho's remnant and SN 1006, believed to be from SNe Ia, are examples of such so-called Balmer-dominated SNRs in the Galaxy. There are also four such remnants in the LMC (Tuohy et al. 1982). Two of them, 0509−67.5, and 0519−69.0, show strong X-ray emission lines of the metals Si, S, Ar, Ca, and Fe (Hughes et al. 1995), which are known to be characteristic of SN Ia ejecta. The young inferred ages of these SNRs ($\lesssim$1500 yr) are consistent with the ejecta-dominated nature of their X-ray emission. DEM 71 is another LMC Balmer-dominated SNR that is older and more evolved than the two just discussed. Based on its age, size, and the estimated amount of gas swept-up by the blast wave (see Table 2), DEM 71 is believed to be in a transition state in which the X-ray emission is changing from being dominated by SN ejecta to being dominated by swept-up interstellar gas. (The fourth LMC example of this class, 0548−70.4, is a much weaker X-ray source and is not in the current *ASCA* sample, so it will not be discussed further.)

The Balmer-dominated optical spectra can be interpreted rather well in the context of a model in which a high-velocity interstellar shock overtakes at least partially neutral interstellar gas (Chevalier & Raymond 1978). When examined in detail, the H$\alpha$ line from these remnants shows a distinctive two-component line profile, consisting of narrow and broad components. The width of the broad component provides a nearly direct measurement of the shock velocity. For DEM 71, Smith et al. (1991) determined a probable range for the shock velocity of 300–800 km $s^{-1}$, which corresponds to shock temperatures of 0.11–0.76 keV. This range is in very good agreement with our X-ray–derived value of $kT_s \sim 0.8$ keV.

It is now reasonably secure that Balmer-dominated SNRs are the remnants of SNe Ia. In light of this point, it is very interesting that DEM 71 is the only remnant in the current *ASCA* sample that shows direct evidence for enhanced abundances. As clearly shown in Figure 4 the iron abundance of DEM 71 is about a factor of 2 higher than all the others in the sample. This corresponds to an amount of "extra" iron present in DEM 71 of roughly $M_{Fe} \sim 0.06$ $M_\odot$, which is about 10% of the total amount of iron believed to be ejected by a Type Ia supernova (Nomoto, Thielemann, & Yokoi 1984). This discovery provides further support for a causal connection between Balmer-dominated SNRs and SNe Ia, and it highlights the importance of such objects for understanding the chemical enrichment of the ISM. Follow-up observations with *AXAF* and searches for coronal [Fe XIV] $\lambda$5303 emission are planned in order to determine the spatial distribution of the excess iron in DEM 71 and to search for other elemental species that might be enhanced.

### 7.5. *N132D*

N132D is the one of the brightest LMC remnants and is probably the best studied of them all. Its popularity with optical observers is due in part to the fact that it contains high-velocity oxygen-rich ejecta that identifies the remnant as having come from the core-collapse SN of a massive star. This ejecta lies near the geometric center of the remnant and is surrounded by a larger limb-brightened shell of material with normal LMC abundances (see references in Morse, Winkler, & Kirshner 1995). These two components also appear, more or less, in the radio (Dickel & Milne 1995) and the X-ray (Hughes 1987) images of N132D, although individual features when examined in detail do vary with wavelength. It is not known if the X-ray–emitting features near the center of the remnant are oxygen rich. One clue, suggesting that they may not be enhanced, was first presented by Blair, Raymond, & Long (1994) who noted that the X-ray peaks near the center were generally associated with low-velocity, normal composition, optical filaments, rather than with high-velocity, oxygen-rich ones. *HST* observations of N132D (Morse et al. 1996) provide a clear confirmation of this effect.

The high-velocity oxygen-rich filaments provide an independent estimate of the age of N132D. The most detailed analysis of the velocity field of N132D has been carried out by Morse et al. (1995) who find an expansion velocity of $\sim$1650 km $s^{-1}$ for filaments with a mean radius of 5.3 pc, which results in a kinematic age of $\sim$3200 yr assuming undecelerated motion. This value is considerably less than the Sedov dynamical age we quote in Table 2. This discrepancy between the kinematic age and the Sedov dynamical age was noted before (Hughes 1987), and it led to the suggestion that N132D exploded within a low-density cavity evacuated by the stellar wind and ionizing radiation of the high-mass progenitor. In this scenario, the outer shell of emission is the main blast wave that has reached the edge of the cavity and is now interacting with the high-density material there. The high density of the ambient medium can be explained by the presence of a giant molecular cloud associated with N132D (Banas et al. 1997). Our work with the *ASCA* spectra provides yet another independent estimate of the age, based on the ionization timescale, which is also considerably less than the Sedov dynamical age and supports the cavity scenario.

Our derived N132D abundances for the elements from oxygen to iron are higher by, at most, a factor of 3 than those derived by Hwang et al. (1993) using data from the *Einstein Observatory*. There are several reasons for this discrepancy. First, our *ASCA* SIS data are of considerably higher quality (in all respects: higher sensitivity, lower background, better spectral resolution, more accurate calibration, and coverage of a broader X-ray band) than the *Einstein* SSS data used by Hwang et al. Our Sedov models provide a more realistic description of the physical conditions in the SNR than the single-temperature single-timescale phenomenological NEI models used previously. The fitted column density in our work is about a factor of 2 more than that of Hwang et al., which tends to increase our

fitted abundances relative to theirs. Note that both our fitted column density and that of Hwang et al. are consistent with the total column of neutral hydrogen toward N132D, $N_{\rm H\,I} \approx 1.4 \times 10^{21}$ cm$^{-2}$. We believe our X-ray determination of the absorbing column density is more accurate because it is based on a more realistic spectral model and because the *ASCA* data are better calibrated in the important band below 1 keV. Additionally, we can point to the excellent correlation we get between the H I column and the X-ray column for the seven SNRs in our sample to support the general accuracy of our results.

Another determination of N132D's abundances was recently presented by Favata et al. (1997) using X-ray spectral data from *BeppoSAX*. The high abundances quoted by these authors are apparently the result of a data analysis error and are spurious (F. Favata 1998, private communication). A revised analysis of the *BeppoSAX* data for N132D yields abundances that are compatible with the values we derive from the *ASCA* data (the 90% confidence intervals overlap). This is an important confirmation, since the revised Favata et al. (1997) analysis is fully independent of ours in that they use a different spectral code, a different model for the temperature and ionization state (a two-component NEI model), and a different set of data. Thus the agreement between the *ASCA* and *BeppoSAX* abundances for N132D, even given these differences, suggests that X-ray–derived abundances from SNRs are quite robust.

### 7.6. *0453−68.5*

This remnant is located in the western edge of the LMC and, like N23 above, is also rather poorly studied. It has been tentatively classified as the remnant of a SN Ia (Population II) by CK88 owing to the lack of nearby OB stars, H II regions, and CO emission. This interpretation is consistent with the low preshock density we derive for 0453−68.5 ($n_0 = 0.30$ cm$^{-3}$, the lowest value in the sample), although a lack of evidence for an overabundance of iron, as seen for DEM 71, is a (weak) countervailing factor. The line-of-sight column density is low, similar to the values found for N23 and DEM 71, and probably arises mostly from the interstellar medium of the Galaxy.

### 7.7. *N49B*

Optically, N49B consists of two sets of bright knots separated on the sky by approximately 1.'4 and embedded in a patchy network of diffuse nebulosity. Its X-ray appearance is entirely different, showing a somewhat limb-brightened, nearly circular region of emission that encompasses both sets of optical knots. On the basis of its location within the H II region DEM 181, CK88 identify N49B with a Populaton I progenitor, a picture that is consistent with our finding that N49B is the result of an explosion within a preexisting cavity in the ISM. The relatively high column density toward this remnant suggests that its association with molecular emission (Cohen et al. 1988) may be more than an accidental projection effect.

## 8. SUMMARY

We have carried out a systematic analysis of the *ASCA* SIS X-ray spectra of seven luminous SNRs in the LMC. Our work has resulted in the following conclusions.

1. The spectral data are described well by a NEI model that includes the time evolution of density and temperature given by the Sedov similarity solution for the dynamical evolution of SNRs. This model was a better description of the data than any single or multiple component phenomenological NEI model that we tried.

2. The X-ray data provide four independent constraints on the three independent parameters of the Sedov model. The observational constraints are radius, shock temperature, emission measure, and ionization timescale. The parameters of the Sedov model are age, initial explosion energy, and ambient ISM density. There is an additional ambiguity in the models that arises from the unknown relationship between the energy imparted to electrons and ions at the shock front. We model two extreme situations: full equilibration (in which the electron and ion temperatures are assumed to be equal) and Coulomb equilibration (in which the electrons gain energy from the ions though Coulomb collisions only).

3. Four of the remnants in the sample, N23, N49, DEM 71, and 0453−68.5, are fully consistent with Sedov evolution under the assumption of Coulomb equilibration. For this group of remnants, the mean explosion energy is $(1.1 \pm 0.5) \times 10^{51}$ ergs, in agreement with the canonical value. The key to discriminating between the full and Coulomb equilibration models comes from comparing the Sedov dynamical age with the age determined from the ionization timescale.

4. When the derived parameters of the other three SNRs, N63A, N132D, and N49B, are examined in detail, they appear to be internally inconsistent. In particular the age determined by the ionization timescale is considerably less than the Sedov dynamical age, regardless of whether one assumes the full or Coulomb equilibration models. Furthermore the initial SN explosion energies are large, $\gtrsim 3 \times 10^{51}$ ergs. Both of these discrepancies can be explained by invoking a scenario in which the remnants exploded within preexisting cavities or bubbles in the ISM and that the X-ray emission we see now comes from the blast wave interacting with the dense material at the cavity wall. This was previously suggested for N132D to explain the discrepancy between this remnant's Sedov age and the kinematic age determined from the expansion of high-velocity oxygen-rich filaments. Our independent estimate of N132D's age from its ionization timescale confirms this earlier result, and it gives confidence that N63A and N49B are actually two more examples of this phenomenon. This result is not particularly surprising since it is precisely the manner in which massive stars are predicted to modify their environment.

5. We find statistical evidence for enrichment by supernova ejecta in the sense that smaller remnants show a somewhat higher mean metallicity than the larger ones. On the other hand, the mean metallicity does not correlate with swept-up mass. In the case of the Balmer-dominated SNR DEM 71, which is likely to be the remnant of a Type Ia supernova, the derived abundance of iron is about a factor of 2 larger than the other remnants in the sample. This corresponds to an excess of iron over the amount in the ISM of $\sim 0.06\ M_\odot$, which is about 10% of the total amount of iron ejected by a Type Ia supernova.

6. All things being considered, however, the middle-aged, evolved SNRs in our sample are in general dominated by swept-up ISM and so can be used to estimate the mean LMC gas-phase abundances. We find that the common elements from oxygen to iron have abundances 0.2–0.4 times solar, consistent with previous results based on optical and UV data, but without the anomalous overabundance of Mg

and Si seen by others. This work demonstrates the validity of using X-ray spectra of SNRs to measure the current chemical composition of interstellar gas, and it has the potential to provide a significant new constraint on the chemical evolution and star formation history of the Cloud.

7. We set limits on the hard ($\gtrsim 3$ keV) X-ray flux of the remnants that correspond to luminosities of from $1.9 \times 10^{35}$ ergs $s^{-1}$ to $2.2 \times 10^{36}$ ergs $s^{-1}$ in the 0.2–4.0 keV band. These limits indicate that the remnants in the sample do not contain very luminous pulsar-powered synchrotron nebulae, as is consistent with our picture of them as evolved middle-aged SNRs. However, the quoted luminosity range is consistent with the possibility that they contain weaker synchrotron nebulae with pulsars losing energy at a slower rate than is the case in the Crab Nebula, for example. The discovery of such a pulsar-powered synchrotron nebula in an LMC SNR would definitively identify the progenitor as a massive star that underwent a core-collapse SN. The expected X-ray luminosities of LMC synchrotron nebulae are easily within the range of detection by *AXAF* and should be pursued.

We gratefully acknowledge the numerous scientists, engineers, and other members of the team that designed, developed, and built *ASCA*. We thank D. Helfand and P. Slane for useful discussions and comments on the manuscript and T. Murakami for allowing us early access to the *ASCA* data on N49. This research has made use of the NASA/IPAC Extragalactic Database (NED) which is operated by the Jet Propulsion Laboratory, California Institute of Technology, under contract with the National Aeronautics and Space Administration. This research was partially supported by NASA grants NAG 5-2684, NAG 5-0638, and NAG 5-4794 and NSF grant INT-9308299 to J. P. H.

## REFERENCES

Allen, C. W. 1973, Astrophysical Quantities (3d ed.; London: Athlone)
Banas, K. R., Hughes, J. P., Bronfman, L., & Nyman, L.-Å. 1997, ApJ, 480, 607
Blair, W. P., Kirshner, R. P., & Chevalier, R. A. 1981, ApJ, 247, 879
Blair, W. P., Raymond, J. C., & Long, K. S. 1994, ApJ, 423, 334
Blanton, E. L., & Helfand, D. J. 1996, ApJ, 470, 961
Chevalier, R. A., & Raymond R. C. 1978, ApJ, 225, L27
Chu, Y.-H., & Kennicutt, R. C. 1988, AJ, 96, 1874 (CK88)
Clark, D. H., Tuohy, I. R., Long, K. S., Szymkowiak, A. E., Dopita, M. A., Mathewson, D. S., & Culhane, J. L. 1982, ApJ, 255, 440
Cohen, R. S., Dame, T. M., Garay, G., Montani, J., Rubio, M., & Thaddeus, P. 1988, ApJ, 331, L95
Cox, D. P. 1972, ApJ, 178, 159
Cox, D. P., & Anderson, P. R. 1982, ApJ, 253, 268
Danziger, I. J., & Leibowitz, E. M. 1985, MNRAS, 216, 365
Davies, R. D., Elliott, K. H., & Meaburn, J. 1976, MmRAS, 81, 89
Dickel, J. R., et al. 1995, ApJ, 448, 623
Dickel, J. R., & Milne, D. K. 1995, AJ, 109, 200
Dickel, J. R., Milne, D. K., Junkes, N., & Klein, U. 1993, A&A, 275, 265
Dopita, M. A. 1979, ApJS, 40, 455
Dufour, R. J. 1984, in IAU Symp. 108, Structure and Evolution of the Magellanic Clouds, ed. S. van den Bergh & K. S. de Boer (Dordrecht: Reidel), 353
Favata, F., Vink, J., Parmar, A. N., Kaastra, J. S., Mineo, T. 1997, AA, 324, L45
Fitzpatrick, E. L. 1985, ApJ, 299, 219
Gull, S. F. 1973, MNRAS, 161, 47
Hamilton, A. J. S., Sarazin, C. L., & Chevalier, R. A. 1983, ApJS, 51, 115
Harrus, I., Hughes, J. P., Helfand, D. J. 1996, ApJ, 464, L161
Harrus, I., Hughes, J. P., & Slane, P. O. 1998, ApJ, 499, 273
Hayashi, I. 1997, Ph.D. thesis, Kyoto Univ.
Hayashi, I., Koyama, K., Hughes, J. P., & Murakami, T. 1995, in UV and X-Ray Spectroscopy of Astrophysical and Laboratory Plasmas, ed. K. Yamashita & T. Watanabe (Tokyo: Universal Academy), 319
Hayashi, I., Koyama, K., Ozaki, M., Miyata, E., Tsunemi, H., Hughes, J. P., & Petre, R. 1994, PASJ, 46, L121
Heiles, C., & Cleary, M. N. 1979, Australian. J. Phys. Astrophys. Suppl., 47, 1
Henize, K. G. 1956, ApJS, 2, 315
Hughes, J. P. 1987, ApJ, 314, 103
Hughes, J. P., et al. 1995, ApJ, 444, L81
Hughes, J. P., & Helfand, D. J. 1985, ApJ, 291, 544
Hughes, J. P., & Singh, K. P. 1994, ApJ, 422, 126
Hwang, U., Hughes, J. P., Canizares, C. R., & Markert, T. H. 1993, ApJ, 414, 219
Israel, F. P., et al. 1993, A&A, 276, 25
Itoh, H. 1978, PASJ, 30, 489
Kobulnicky, C. 1997, in ASP Conf. Ser. 147, Abundance Profiles: Diagnostic Tools for Galaxy History, ed. D. Friedli, M. Edmunds, C. Robert, & L. Drissen (San Francisco: ASP), 108
Koyama, K., et al. 1995, Nature, 378, 255
Kulkarni, S. R., Frail, D. A., Kassim, N. E., Murakami, T., & Vasisht, G. 1994, Nature, 368, 129
Laming, J. M., Raymond, J. C., McLaughlin, B. M., & Blair, W. P. 1996, ApJ, 472, 267
Luck, R. E., & Lambert D. L. 1992, ApJS, 79, 303
Marshall, F., et al. 1998, IAU Circ. 6810
Masai, K. 1984, Ap&SS, 98, 367
Mathewson, D. S., Ford, V. L., Dopita, M. A., Tuohy, I. R., Long, K. S., & Helfand D. J. 1983, ApJS, 51, 345
Mathewson, D. S., Ford, V. L., Dopita, M. A., Tuohy, I. R., Mills, B. Y., & Turtle A. J. 1984, ApJS, 55, 189
Mathewson, D. S., Ford, V. L., Tuohy, I. R., Mills, B. Y., Turtle A. J., & Helfand, D. J. 1985, ApJS, 58, 197
Mathis, J. S. 1990, ARA&A, 28, 37
McGee, R. X., & Milton, J. A. 1966, Australian J. Phys., 19, 343
McKee, C. F. 1974, ApJ, 188, 335
Morrison, R. & McCammon, D. 1983, ApJ, 270, 119
Morse, J. A., et al. 1996, AJ, 112, 509
Morse, J. A., Winkler, P. F., & Kirshner, R. P. 1995, AJ, 109, 2104
Murakami, T., Tanaka, Y., Kulkarni, S. R., Ogasaka, Y., Sonobe, T., Ogawara, Y., Aoki, T., & Yoshida, A. 1994, Nature, 368, 127
Nomoto, K., Thielemann, F.-K., & Yokoi, M. 1984, ApJ, 286, 644
Rothschild, R. E., Kulkarni, S. R., & Lingenfelter, R. E. 1994, Nature, 368, 432
Russell, S. C. & Bessell, M. S. 1989, ApJS, 70, 865
Russell, S. C. & Dopita, M. A. 1990, ApJS, 74, 93
———. 1992. ApJ, 384, 508 (RD92)
Ryter, C., Cesarsky, C. J., & Audouze, J. 1975, ApJ, 198, 103
Sedov, L. I. 1959, Similarity and Dimensional Methods in Mechanics (New York: Academic)
Seward, F. D., Harnden, F. R., & Helfand, D. J. 1984, ApJ, 287, L19
Seward, F. D., & Wang, Z.-R. 1988, ApJ, 332, 199
Shklovsky, I. S. 1968, Supernovae (New York: Wiley-Interscience)
Shull, P. 1983, ApJ, 275, 592
Shull, P., Dyson, J. E., Kahn, F. D., & West, K. A. 1985, MNRAS, 212, 799
Slane, P. O., Seward, F. D., Bandiera, R., Torii, K., & Tsunemi, H. 1997, ApJ, 485, 221
Smith, R. C., Kirshner, R. P., Blair, W. P., & Winkler, P. F. 1991, ApJ, 375, 652
Spitzer, L., Jr. 1978, Physical Processes in the Interstellar Medium (New York: Wiley-Interscience)
Tanaka, Y., Inoue, H., & Holt, S. S. 1994, PASJ, 46, L37
Tenorio-Tagle, G. 1996, AJ, 111, 1641
Thielemann, F.-K., Nomoto, K., & Hashimoto, M. 1996, ApJ, 460, 408
Tsujimoto, T., Nomoto, K., Yoshii, Y., Hashimoto, M., Yanagida, S., & Thielemann, F.-K. 1995, MNRAS, 277, 945
Tuohy, I. R., Dopita, M. A., Mathewson, D. S., Long, K. S., & Helfand, D. J. 1982, ApJ, 261, 473
Vancura, O., Blair, W. P., Long, K. S., & Raymond, J. C. 1992, ApJ, 394, 158
Vancura, O., Raymond, J. C., Dwek, E., Blair, W. P., Long, K. S., and Foster, S. 1994, ApJ, 431, 188
Vasisht, G., Aoki, T., Dotani, T., Kulkarni, S. R., & Nagase, N. 1996, ApJ, 456, L59